VOL. XII - Nº 3 1990 ISSN 0100-7386

# REVISTA BRASILEIRA DE CIÊNCIAS MECÂNICAS

JOURNAL OF THE BRAZILIAN SOCIETY OF MECHANICAL SCIENCES

PUBLICAÇÃO DA ABCM
ASSOCIAÇÃO BRASILEIRA DE CIÊNCIAS MECÂNICAS

REVISTA BRASILEIRA DE CIÊNCIAS MECÂNICAS
JOURNAL OF THE BRAZILIAN SOCIETY OF MECHANICAL SCIENCES



Publicado pela / Published by

ASSOCIAÇÃO BRASILEIRA DE CIÊNCIAS MECÂNICAS, ABCM /
BRAZILIAN SOCIETY OF MECHANICAL SCIENCES

Secretária da ABCM: Sra. Simone Maria Frade
Av. Rio Branco, 124 - 18º Andar - Rio de Janeiro - Brasil
Tel. (021) 221-6177 R. 278, Telex (21) 37973 CGEN-BR

Presidente: Sidney Stuckenbruck
Secret. Geral: Eloi Fernandez y Fernandez
Diretor de Patrimônio: Antonio MacDowell de Figueiredo

Vice-Presidente: Luiz Bevilacqua
Secretário: Oswaldo A.Pedrosa Jr.

PROGRAMA DE APOIO À PUBLICAÇÕES CIENTÍFICAS

MCT

CNPq

finep

**RBCM – J. of the Braz.Soc.Mech.Sc.** ISSN 0100-7386
*Vol.XII - nº 3 - pp. 227-252 - 1990* Impresso no Brasil

# AN ANALYSIS OF CURRENT MODELS FOR TURBULENT JETS IN CROSS-FLOWS

## *UMA ANÁLISE DOS MODELOS PARA JATOS TURBULENTOS EM ESCOAMENTO CRUZADO*

**Sérgio Luis Villares Coelho**
Laboratório de Mecânica dos Fluidos-Aerodinâmica
Programa de Engenharia Mecânica – COPPE/UFRJ
C.P. 68.503
21945 Rio de Janeiro, RJ - Brasil

### ABSTRACT

*A review and a discussion of the models which have been used to explain and simulate various aspects of jets issuing into uniform cross-flows are presented. Some aspects of these models are here analysed and compared with recent analytical results for the near field of these flows. The flow in this region allows for a rather rigorous analysis of the mechanics involved in the distortion and deflection of the jet, and also in the formation of the pair of trailing vortices. It is found by this analysis that turbulent entrainment and the transport of the transversal component of vorticity have strong influence on the dynamics of the mixing layer in the initial region of the jet. These findings and further considerations on the formation of the wake behind the jet lead to two main conclusions: (i) The deflection of the jet in the near field of these flows is mainly due to entrainment rather than to pressure drag: (ii) The transversal component of vorticity has a strong influence on the formation of the pair of trailing vortices, inducing a rapid transference of transversal vorticity into the pair of vortices which is being formed.*

**Keywords:** Jets ▪ Turbulent Jets ▪ Jet Wakes

### RESUMO

*Uma revisão e discussão dos modelos que têm sido usados para explicar e simular vários aspectos de jatos emergindo em escoamentos uniforme e cruzado são apresentados. Alguns aspectos destes modelos são aqui analisados e comparados com resultados analíticos recentes para o escoamento nas redondezas do jato. É observado na presente análise que o entranhamento turbulento e o transporte da componente transversal da vorticidade têm forte influência na dinâmica da região de mistura na parte inicial do jato. Tais descobertas e considerações adicionais sobre a formação da esteira na parte posterior do jato conduzem a duas conclusões principais: (i) A deflexão do jato no escoamento principal se deve principalmente ao entranhamento de massa e não ao arraste associado à pressão. (ii) A componente transversal da vorticidade tem forte influência na formação do par de vortices que são carregados pelo escoamento, induzindo uma rápida transferência da vorticidade transversal para o par de vórtices que se forma.*

**Palavras-chave:** Jatos ▪ Jatos Turbulentos ▪ Esteiras de Jatos

Submetido em Abril/89 Aceito em Novembro/89

## INTRODUCTION

The issuing of jets into deflecting streams has been the subject of numerous studies because of its wide variety of applications in engineering. Chimney plumes for the dispersion of polutants in the atmosphere, the cooling of turbine blades, lifting jets for V/STOL aircraft and jets of oil and gas entering the flow in oil wells are just a few of the important examples.

Despite the many practical fluid mechanics problems where solutions depend on understanding the behaviour of jets, questions of how and why turbulent jets bend over when they enter cross streams have not yet been satisfactorily answered. Quite different answers to these questions have been given in different fields of application. These are based on different explanations of the mechanics of the flow! Furthermore, few attempts to describe the formation of the trailing vortex pair, which is a characteristic of these flows, have been made.

These facts reduce one's confidence in the current basis of the many models which are based on these different explanations. It is important that there is a basic understanding of the mechanisms that govern the motion of simple turbulent jets issuing normally to uniform cross-flows before one can have confidence in the use of current models for jet flows in more complex situations.

In this paper, a review and a discussion of the models which have been used to explain and simulate various aspects of jets issuing into uniform cross-flows are presented. Some aspects of these models are here analysed and compared with recent analytical results for the near field of these flows. The flow in this region allows for a rather more rigorous analysis of the mechanics involved in the distortion and deflection of the jet, and also in the formation of the pair of trailing vortices. It is found by this analysis that turbulent entraiment and the transport of the transversal component of vorticy have strong influence on the dynamics of the mixing layer in the initial region of the jet.

These findings and further considerations on the formation of the wake behind the jet lead to two main conclusions: (i) The deflection of the jet in the near field of these flows is mainly due to entrainment rather than to pressure drag. (ii) The transversal component of vorticity has a strong influence on the formation

of the pair of trailing vortices, inducing a rapid transference of transversal vorticy into the pair of vortices which is being formed.

## EXPERIMENTAL INVESTIGATION OF THE FLOW

Experimental observations (e.g. [1], [2] and [3]) provide the following overall description for the flow induced by the issuing of a turbulent incompressible non-buoyant circular jet from a plane wall into a deflecting stream with a uniform velocity profile (schematically shown in Figure 1): in the region near the issuing nozzle (near-field) the initially circular cross-section of the jet is deformed into an "ellipsoidal" shape which is symmetric with respect to the $x$ direction (see Figure 1), but slightly non-symmetric with respect to the $y$ direction. Turbulence develops along the boundaries of the jet because of the velocity excess in this region of the flow and, consequently, fluid from the external stream is entrained by the jet, leading to an increase in its cross-sectional area and a change in the velocity distribution over its cross-section. This turbulent region is a turbulent mixing layer that grows thicker, entraining fluid from the external stream and eating up the inner region were the flow is still non-turbulent (the potential core). Despite the fact that the cross-section grows non-symmetrically with respect to the $y$ direction, characterizing a deflection of the jet in the direction of the stream, the potential core is not deflected even for relatively low ratios $\alpha = U_j/U_\infty$ ([4] reports no downwind shift of the potential core for $\alpha > 4$). At the region about the end of the potential core the flow is characterized by a horse-shoe shape assumed by the cross-section of the jet and most of the downwind deflection occurs in the region just after the end of the potential core. At this stage the jet is fully turbulent and a pair of contra-rotating vortices begins to be evident in the downwind side of the plume, apparently being formed due to a roll-up process that occurs on the trailling edges of the horse-shoe shaped cross-section. In the far-field (several jet diameters downstream) practically all the fluid within the jet is concentrated in a pair of vortices that approach asymptotically the direction of the free stream. Figure 1 also shows photographs for each of these stages of the flow (the experimental technique used to obtain these photographs is outlined in [5]).

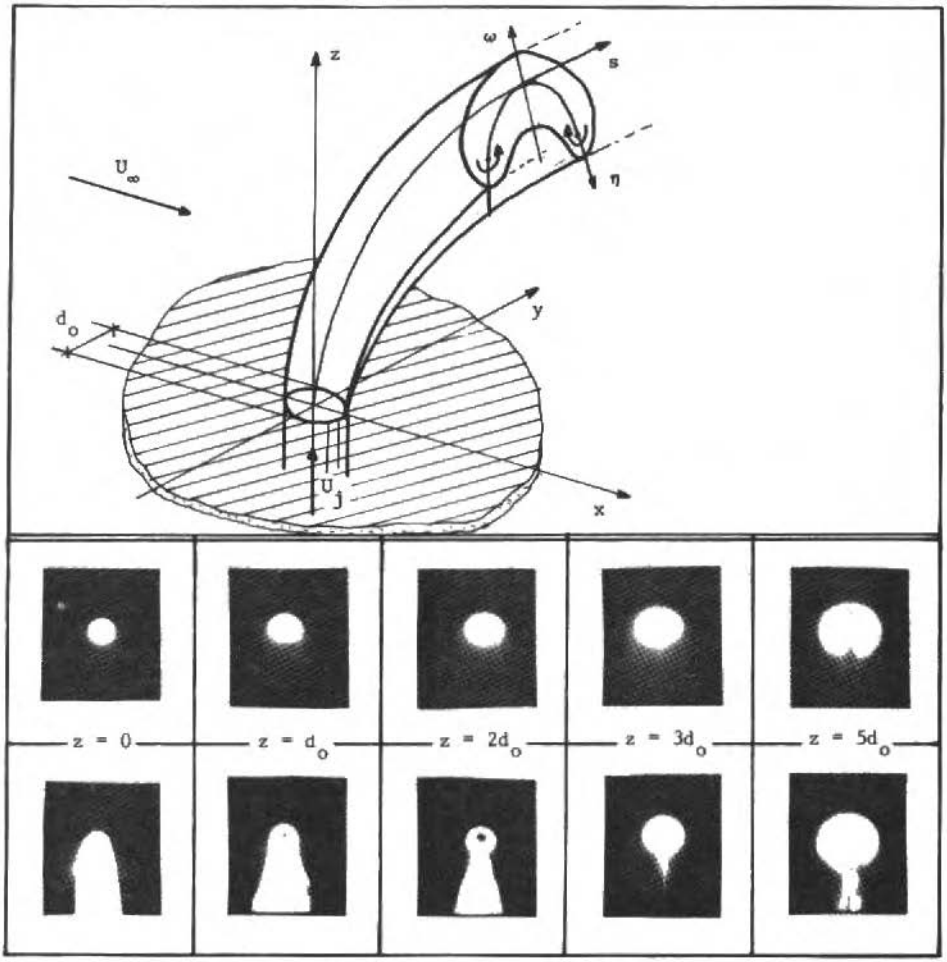


Figure 1. Schematic view of a jet in a uniform cross-flow. Top line photographs show cross-sections for a jet of smoke in air stream and bottom line photographs show the growth of the potential core.

The description given above is only valid beyond a certain value for $\alpha$ since for low velocity ratios the jet is pusched too quickly in the direction of the strong stream, altering completely the pattern of the flow. So, this description

is restricted to the case of "strongs" jets. The word "strongs" is used here in the same sense as [6] defined strong and weak jets. Following topology considerations by [7], Foss defined jets as strong or weak depending upon the position of the net saddle point in the external flow about the initial region of a round jet issuing from a wall. Using surface streaking techniques and dye, Foss obtained the flow patterns for 14 different values of $\alpha$ in the interval $.1 < \alpha < 3.17$ and observed that for a weak jet there is only one saddle point positioned ahead of the jet. When the velocity ratio is increased beyond a certain value the exceeding saddle in the saddle-node patterns is always positioned downstream from the jet. According to Foss this transition occurs at $\alpha \simeq .5$ and "appears to be related to the increase in the jet stiffness whereby the jet fluid at the aft side of the hole penetrates a substantial distance into the cross-stream before being deflected". Thus, the word "strong" is used here to characterize flows for which their general pattern is similar to those flows with high values for $\alpha$. It is worth mentioning that, since turbulence is the dominant diffusion mechanism in most of the real jet flows, flows with low Reynolds numbers are not being considered in this work.

Experiments concerning many different aspects of jets issuing into cross-flows have been conducted in the past fourty years. Callaghan & Ruggeri [8] carried out one of the first experiments with these flows and evaluated the penetration depth for a round heated jet of air issuing into a uniform cross-flow by measuring temperature distributions. Jordinson [9] evaluated the trajectory of a round jet issuing perpendicularly into a deflecting stream by measuring the distribution of the total pressure (stagnation pressure) along six transversal planes accross the plume. The trajectory of the jet was defined as the line of maximum total head along the plane of symmetry of the flow. In this work, Jordinson also presents the total pressure distributions which were obtained for each of the six transversal planes. Keffer & Baines [4] carried out an extensive experimental work with circular jets issuing into cross-flows. Defining the jet centerline as the locus of maximum velocity along the plane of symmetry, curves for this centerline were obtained for five ratios of $\alpha(\alpha = 2, 4, 6, 8,$ and $10)$. They also observed that the mean velocity distributions along transversal planes are approximately similar with respect to a natural system of coordinates ($\omega$ and $\eta$ in Figure 1) in the region where the effects of the trailing vortices are still limited. Measurements of the velocity distribution over transversal planes for this same jet configuration were also carried out by [10]. Contours of constant

velocity, constant temperature (for heated jets) and contours of constant turbulence intensities for selected transversal planes are presented in their paper for $\alpha \simeq 15$ and $\alpha \simeq 60$. Experimental data for the turbulence fields of jet flows has also been obtained by [11] for $\alpha = .5$, 1 and 2. Additional information on these fields has been recently obtained by [12] and [13]. Unfortunatelly these measurements are for a velocity ratio of $\alpha = .5$ (the transition region according to Foss), not revealing much about the patterns of turbulence fields for strong jets.

Experiments especifically concerning the initial region of the jet have been also performed and a few results published in the literature. Fearn & Weston [14] measured the static pressure distribution over the plane surface from which a round jet was issued into a uniform cross-stream for values of $\alpha$ ranging from 2 to 10 and for jet Mach numbers ranging from .09 to .95. Their results for low Mach numbers could well be compared with pressure distributions for incompressible jets. Thompson [15] has also measured this pressure field for $\alpha = 2, 4$ and 8 with low Mach numbers. Moussa et al. [16] measured velocity and vorticity distributions in the near-field of round jets in cross-flows and obtained contours for each component of the velocity and vorticity vector fields for $\alpha = 3.84$.

The wake formed behind strong jets have also been experimentally studied: McMahon et al. [17] observed that vortex shedding occurs in the wake of turbulent jets and measured these frequencies for a round jet issuing from a wall for $\alpha = 8$ and $\alpha = 12$. They found that when the initial diameter of the jet is used in the definition of the Strouhal number for these flows the values obtained are less than one half of the typical value for a solid cylinder in a uniform flow ($S = .21$). Considering that the initial diameter is not an appropriate dimension to be taken as the effective length scale in the definition of this number, since the jet grows and distorts as it leaves the plane, they observed that a "proper value" of 2.2 diameters "yields a value of Strouhal number consistent with the solid cylinder". However, experimental data obtained by [16] for this same flow configuration show a sharp decrease in the values for the Strouhal number (based on this initial diameter) as $\alpha$ increases! This seems to support the idea of [9] that the flow around the initial region of the jet "may be similar to the flow over a porous cylinder with suction" and not to the flow around a solid cylinder. From experimental measurements carried out

by [18], [19] evaluated the drag on a circular cylinder with a Thwaite's flap as a function of suction intensity; it is shown by his results that presure drag falls with the increase of suction until vorticity shedding is completely avoided. Suction reduces the amount of vorticity shed from the cylinder, determining a narrower wake behind the body. Similar behavior should be expected in the absense of the flap, and the only difference would be that in this case vortex shedding would occur, and a higher drag would be experienced for a given suction intensity. Thus, if the initial region of a circular jet is compared with the cylinder with suction, a decrease in the conventional Strouhal number should be expected as the velocity ratio $\alpha$ increases, i.e., as suction increases. Turbulent entrainment would have then sensible effects on the vortex shedding process for jets issuing into cross-flows. This seems to be very much in agreement with the results obtained by [16]. Moussa et al. also evaluated experimentally Strouhal numbers for jets issuing from a pipe into a cross-stream in the absense of a plane wall. In this case they found that the Strouhal number is practically independent of the ratio $\alpha$, assuming a slightly lower value than that for a solid cylinder (when the initial diameter is taken as the lengh scale for the Strouhal number). It seems that in this case the vortex shedding from the pipe governs the vortex shedding process, determining the frequency at which vortices are shed from the jet.

## MATHEMATICAL MODELS FOR THE JET

Mathematical models for the issuing of jets into cross streams based on completely different approaches have been presented in the literature. In environmental fluid mechanics the jet flow is usually modelled by an integral approach, where an entraining control surface is assumed for the jet; aerodynamicists have also used integral approaches, modelling the flow as a pair of contra-rotating vortex-filaments or tubes in a cross stream (Figure 2). Satisfactory agreement with experimental data for the trajectory of the jet has been reported with both approaches.

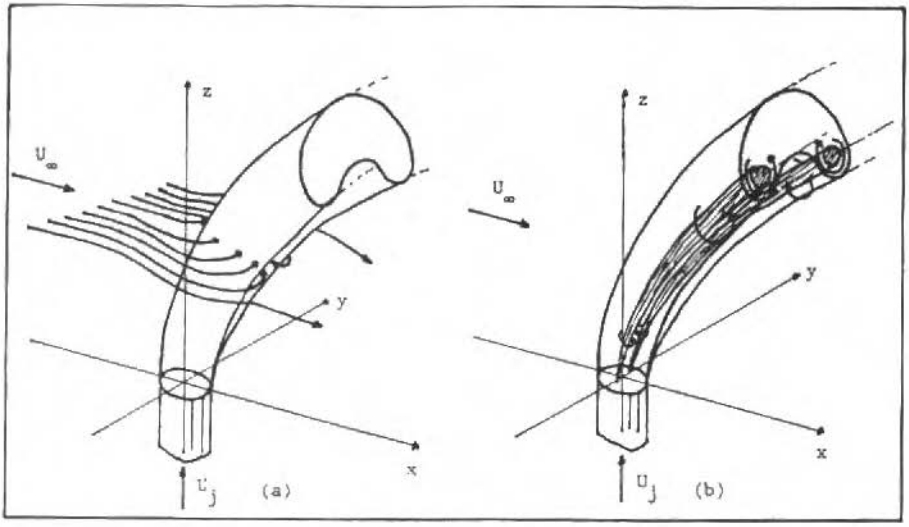


Figure 2. Models for a jet in a cross-flow: (a) entraining surface; (b) vortex pair.

Most of the mathematical models which have been proposed for jets in cross flows have been mainly concerned with the evaluation of the trajectory and the approximate size of the jet. Unfortunatelly, there has not been much agreement between researchers with respect to which physical mechanisms significantly contribute to deflect the jet in the direction of the stream. Jordinson [9] suggested that pressure drag and addition of momentum due to entrainment were the important mechanisms. Nevertheless, [20] assumed that the only driving mechanism is the addition of momentum due to entrainment and considered a constant pressure distribution in their integral formulation for a jet issuing at various angles into a uniform deflecting stream. The closure relations for the fluxes of mass and momentum and the rate of spreading of the plume which are needed when a integral formulation is used were provided by assuming self-preservation and by assuming an entrainment function which depends on coeffcients obtained experimentally. The results obtained for the trajectory agree with experimental data for a wide range of issuing angles. However, [21] assumes that pressure drag is the important mechanism for the jet's shift and completely neglects the effects of the transversal component of

the added momentum. Self-preservation and an entrainment function similar to that one used by Platten & Keffer are also assumed and again fair agreement with experimental data is obtained for the predicted trajectory.

Several other integral models have been developed for the deflection of the jet and most of them also show satisfactory predictions for its trajectory. Sucec & Bowly [22] also assumed that the deflection of the jet is due to the action of pressure drag forces, neglecting, like Endo, the addition of "transversal momentum" to the plume by means of turbulent entrainment. Information concerning the rate of spread of the jet was inputed into their model via empirical relations obtained by [23] and the velocity profiles were assumed to be similar to those for a planar jet with a co-flowing stream. Again, suitable values for the empirical constants provide satisfactory predictions for the trajectory of the jet. Makihata & Miyai [24] also assume pressure drag as the mechanism that drives the flow and take Gaussian distributions for the velocity profiles. An entrainment function is assumed and again satisfactory prediction for the trajectory is achieved with their model. In his comprehensive integral model for the plume rise [25] considered presure drag and addition of momentum as the important mechanisms for the trajectory of non-buoyant jets (according to this particular case in his general equations for buoyant jets in stratified cross streams). A much more elaborated entrainment function than the one assumed by Platten & Keffer is derived from the mean kinetic energy equation but, once more, Gaussian distribution for velocity profiles is assumed. Again, fair predictions for the trajectory of the jet are obtained.

In all the above mentioned integral models, the integration of the equations of motion is perfomed assuming circular, ellipsoidal or even rectangular shapes for the cross-section of the jet. This assumption of simplified shapes lead to pressure drag coefficients which lack physical meaning since these are characteristic of the form of the cross-section. Sucec & Bowley integrate their equations over a rectangular cross-section and find good trajectory prediction using $C_d = 1$, for $\alpha > 4$. Makihata & Miyai assume a circular cross-section when integrating their equations and use $C_d = 2$, for $\alpha > 4.4$. Twice the anterior value! As a matter of fact, Makihata & Miyai comment the wide range of values for the pressure drag coeffcient which has been used by researchers in their integral models: these range from 1 to 3! This is very much in disagreement with the idea of comparing the jet with a bluff body with suction

since, for this case, the value of the drag coefficient should be lower than the corresponding value for the solid body case. $C_d = 2$ or higher values seem to be very unexpected for a initially circular jet if it is recalled that $C_d = 2.05$ is the typical value for a square solid cylinder in a cross stream for $10^4 < \text{Re} < 10^6$ [19]. It should be also recalled that the subcritical pressure drag coefficient for a solid circular cylinder in a cross flow is always lower than 1.2 for Re> 300 [26].

Adler & Baron [27] have evaluated the shape of the cross-section via a two-dimensional time dependent vortex-sheet model introduced by [28] and considered these shapes in their numerical integration. Two mechanisms, pressure drag and added momentum, are taken into account. However, the value used for $C_d$ is the same as for a solid cylinder and the "more realistic" shapes for the cross-sections are not taken into account in the determination of this parameter. Nevertheless, satisfactory results are still obtained for the trajectory of the jet.

The results obtained with the above mentioned integral models show that similar behaviours for the trajectory of the jet seem to be predicted even when completely different mechanisms are assumed as being the driving ones for these flows. Thus, the mere fact that an integral model for the jet gives good results for its trajectory does not imply that the assumptions made are "fullfiled" by real jets.

The reason why integral models seem to predict reasonably well the trajectory of jets in cross-flows regardless of the assumptions made with respect to the mechanisms reponsible for the deflection of the jet becomes apparent with the following analysis: the local change in the trajectory of the jet shown in Figure 3 is determined by the rate of change of the transversal component of the momentum flux along the trajectory of the jet. This change is caused by two different mechanisms: firstly, pressure drag due to a non-symmetric pressure distribution around the jet "pushes" the jet in the transversal direction, changing its trajectory; secondly, the fluid which is entrained by the jet has a non-zero component of "transversal momentum" which is "added" to the jet.

A relation for the local curvature determined by these two mechanisms can be written as (refering to Figure 3, all variables scaled with to $U_j$, $R_0$ and $\rho$):

$$\frac{d\phi}{ds} = \frac{\frac{1}{2}\, C_d\, b(s,\alpha)\, \alpha^{-2}(\sin\phi)^2 + E(s,\alpha)\, \alpha^{-1} \sin\phi}{\int_A u_s^2\, dA} \qquad (1)$$

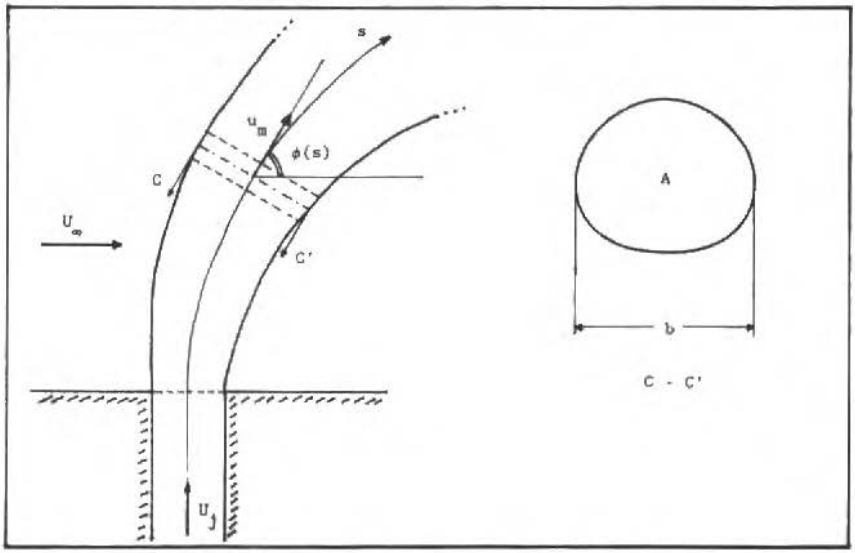


Figure 3. Nomenclature for an element of the jet.

where $b(s,\alpha)$ is the breadth of the jet and $E(s,\alpha)$ is the total local entraining flux. The two components on the top of the right hand side of equation (1) represent the rate of change in the transversal component of the momentum of the fluid element shown if Figure 3, $(dm_t/ds)$, due to the action of pressure drag, $(dm_t/ds)_p$, and due to addition of momentum in the transversal direction, $(dm_t/ds)_e$, respectively. Thus, as long as the functions assumed for $b(s,\alpha)$ and $E(s,\alpha)$ are similar, *any* combination of coefficients which provides similar behaviour for the sum of these two components would reasonably well describe the trajectory of the jet. This can be illustrated with the entraining function assumed by [20]:

$$\frac{E(s,\alpha)}{C_f\, b(s,\alpha)} = C_1(u_m - \alpha^{-1}\cos\phi) + C_2\, \alpha^{-1}\sin\phi\ , \qquad (2)$$

where $C_f$, $C_1$ and $C_2$ are coeffcients; they have experimentally obtained $C_1$ and $C_2$ by fitting the trajectory given by this model to experimental data, obtaining $C_1 = .07$ and $C_2 = .25$. Approximating $E(s,\alpha)$ by

$$E(s,\alpha) \simeq C_e\ b(s,\alpha)\ \alpha^{-1} \sin\phi\ , \tag{3}$$

since $C_2 \gg C_1$, expression (1) can be reduced to:

$$\frac{d\phi}{ds} = \left(\frac{1}{2}\ C_d + C_e\right)\ b(s,\alpha)\ \alpha^{-2}(\sin\phi)^2 \tag{4}$$

and any pair of coefficients with the same sum provides the same trajectory for the jet. As a matter of fact, the behaviours of $b(s,\alpha)\ \alpha^{-2}(\sin\phi)^2$ and $E(s,\alpha)\ \alpha^{-1}\sin\phi$ are somewhat similar when $b(s,\alpha)$ and $E(s,\alpha)$ are obtained from experimental correlations: [29] obtained $b \propto \alpha^{2/3}\ s^{1/3}$, and [30] obtained $E \propto s^{.22}$. These correlations give:

$$(dm_t/ds)_p \propto \alpha^{-1}(\cos\phi)^{.39}(\sin\phi)^{1.61}\ , \tag{5}$$

and

$$(dm_t/ds)_e \propto \alpha^{-.78}(\cos\phi)^{.26}(\sin\phi)^{.74}\ . \tag{6}$$

These expressions are indeed somewhat similar, and their behaviours are graphically shown in Figure 4. Therefore, for any given range of the jet trajectory, suitable constants multiplying (5) and (6) can always be found in such a way that either (5), (6) or the sum of both show "satisfactory agreement" with experimental data.

Models for the jet based on the characteristic trailing vortices (e.g., [31], [32] and [33]) have also been published in the literature. These model the jet as a pair of contra-rotating vortex tubes or filaments and apply, in principle, only to the region where the vortices are dominant, i.e., far from the initial region of the jet. However, [34] extended the validity of their model to the initial region of the jet and used the conditions at the nozzle as initial conditions of their model, where the trajectory of the jet is parameterized with respect to time. No formal analysis is presented to support this extension of validity in their model. This parameterization with respect to time is assumed in all vortex filaments or vortex tubes models and a two-dimensional time evolving approximation is used to determine the "movement" of the filaments or tubes from the forces

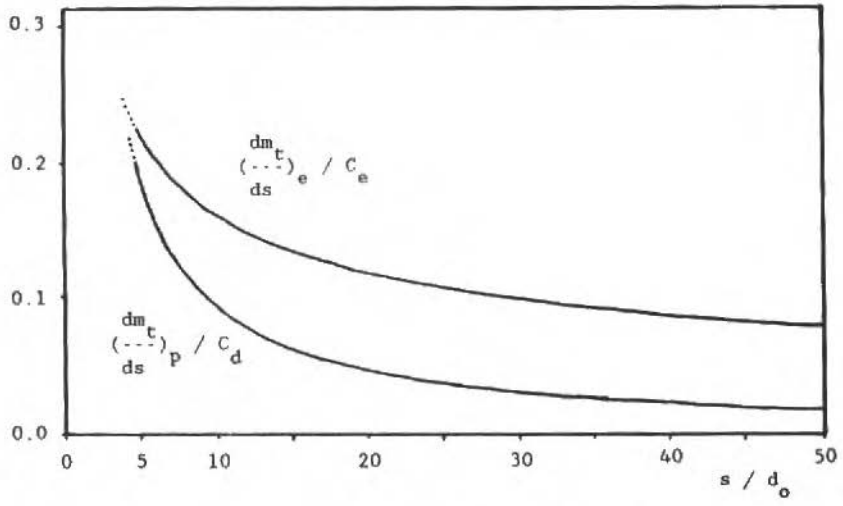


Figure 4. Curves for pressure drag, $(dm_t/ds)_p$, and addition of "transversal momentum", $(dm_t/ds)_e$, along the trajectory of the jet, according to expressions (5) and (6), for $\alpha = 10$.

which are exerted on their cores by this "two-dimensional flow". So, according to these models, pressure drag is the mechanism responsible for the deflection of the jet. In this case, however, pressure drag is assumed to be independent of the entrainment parameters, being a function of the dynamic interaction between the vortex filaments or tubes only. This is a direct consequence of neglecting the effects of entrainment on the size and spacing of the vortex cores. Predictions for the trajectory of the jet produced by these models agree reasonably well with experimental data.

The results obtained with the above mentioned models show that similar trajectories for the jet seem to be predicted even when completely different mechanisms are assumed as being the driving ones for these flows. The lack of full comparison of the flow predicted by these models with experimental data leads to no conclusion at all with respect to the mechanisms which are responsible for the deflection, distortion and formation of the trailing vortex pair of the jet.

## NUMERICAL SIMULATION OF THE FLOW

Numerical solutions for the mean velocity field using the Reynolds equations with the shear stress approximated by some turbulence closure model have been also published in the literature. A high resolution computation of the flow induced by the issuing of a circular jet into a uniform cross stream has been recently carried out by [34] for three velocity ratios ($\alpha = 2, 4$ and 8). Neverthless, even this high resolution computation (the highest so far published) still uses a coarse mesh if one compares the mesh scale ($d_0/2.5$ in this case) with the thickness of the mixing layer in the near field of the flow. Their analysis of the numerical solutions obtained with a $k - \varepsilon$ model for turbulence certainly leads to some insight into the process of the formation of the contra-rotating trailing vortices. However, statement like "the vortex pair is really no more than the original streamwise vorticity in the sides of the jet, and the transverse component is diffused away in the ends of the loop" only to the far field of the flow, and do not describe the dynamics of the vorticity in the near field. If this was so, the total circulation of the trailing vortices would be independent (or slightly dependent, considering difusion) on the velocity ratio $\alpha$, being a function of the external stream velocity and the initial diameter only. Experimental data from [35] show, however, that there is a strong dependence of this local circulation on the velocity ratio $\alpha$. This suggests that the transversal component of vorticity plays an important role on the formation of the trailing vortex pair.

Previous theoretical investigations on the formation of the vortex pair have been based on the time evolving two-dimensional vortex-sheet model introduced by [28]. In these models, the flow in the jet and outside the jet are regarded to be potential flows and the boundary between them to be a vortex-sheet. The additional hypothesis that the form of the three-dimensional vortex-sheet can be approximated by a two-dimensional vortex sheet that evolves in time is made and simple conditions assumed for the nozzle are used as initial conditions.

Discretizing the vortex-sheet into a number of vortex filaments that are essentially aligned with the trajectory of the jet, [36] evaluated the cross-sectional distortion via a numerical computation of the movement of these vortex filaments. Similar evaluations were also carried out by [23] and [37]. The transport of vorticity predicted by these models causes vorticity to concentrate

on the downwind side of the vortex-sheet, leading to a roll-up process that reflects some of the qualitative features present in real jets. However, according to these models, the vortex pair is formed by the concentration of the streamwise component of vorticity only, and the transversal component has no effect in this process. This lead to a total circulation which is independent of the velocity ratio; again, there is a clear disagreement with the experimental data from [35].

The probable reasons for the disagreement between these models and detailed measurements are that turbulent entrainment is ignored, and that a two-dimensional approximation is assumed for a fully three-dimensional vortex-sheet problem. It is worth mentioning that the validity of this two-dimensional approximation for the fully three-dimensional problem appears to be based on intuitive arguments only and no formal analysis to support it has been presented in the literature.

## THE NEAR FIELD OF A STRONG JET IN A UNIFORM CROSS-FLOW

A new asymptotic analysis of the initial region of a strong jet issuing into a uniform cross-flow is presented in [5]. The flow in this region allows for a much more rigorous analysis of the mechanisms involved in the deflection and distortion of the jet, and also in the formation of the pair of trailing vortices. In the initial region, the deflection and distortion of the jet are still small, entrainment is still limited to a thin mixing layer on the boundary of the plume, and the vortex pair is still beginning to be formed. The inviscid three-dimensional vortex-sheet model which is developed produces symmetrical deformations of the jet only. This shows that inviscid mechanisms alone are not able to explain the deflection of the jet in the direction of the stream. In fact, there is nothing to brake the symmetry in the boundary value problem constructed with the inviscid three-dimensional flow hypothesis.

Chang-Lu's model does predict a deflection of the jet but it is valid only in the far field of the flow. When this model is rectified to allow for the three-dimensionality of the near field (the three-dimensional vortex-sheet model), essential features of the initial development of the jet are not reproduced. In particular, the jet does not move downwind.

This result, and the fact that the deflection of the potential core has only been observed for relatively low ratios $\alpha$ [3], support the idea that the effects of pressure drag, which indeed occurs because of the formation of a turbulent wake behind the jet, are negligible when compared to those of entrainment.

As a matter of fact, [38] in his paper on the flow induced by jets recalls that "The sudden change in flow velocity at the cut in the theoretical flow which idealizes the action of the jet on the surrounding fluid seems to be more nearly related to a sheet of sinks than to a sheet of vortices".

Indeed, when a sheet of sinks is added to the three-dimensional vortex-sheet the combined effects of entrainment and the three-dimensional vorticity dynamics of this "entraining vortex-sheet" seem to provide a good description of the flow in the near field of the jet flow.

The transport of the transversal component of vorticity from the upwind side to the downwind side of the jet induces larger velocities on its downwind side, tilting the vorticity lines in the bounding shear layer. This leads to a net transference of vorticity from the transversal direction to the longitudinal direction. The combination of this process with the convection of "longitudinal vorticity" to the downwind side of the plume produces an increasing concentration of longitudinal vorticity on this side which leads to the formation of the vortex pair.

The sink-sheet introduced (to account for entrainment) has a significant effect on the dynamics of the bounding shear layer and provides the asymmetric component of deformation which leads to the deflection of the jet in the direction of the stream.

The shape of the cross-sections of strong round jets at different (small) distances from the exit are described by (see Figure 5; variables scaled with respect to $U_j, R_0$ and $\rho$):

$$R_j = 1 - [k\ z]\,\varepsilon - [Z(z)\cos 2\theta]\,\lambda^2 + O(\lambda^3, \varepsilon^2, \lambda^2\varepsilon) \tag{7a}$$

$$R_e = 1 + [(2+k)\ z]\,\varepsilon + [2(1+k)\,z^2\cos\theta]\,\lambda\varepsilon - [Z(z)\cos 2\theta]\,\lambda^2 + O(\lambda^3, \varepsilon^2, \lambda^2\varepsilon) \tag{7b}$$

where $\lambda = 1/\alpha$, $\varepsilon$ is the entrainment coefficient for a free turbulent jet in a stangnant external flow, $k = O(1)$ is a constant relating $v_{en}$ and $v_{jn}$ (see Figure 5) such that $v_{en} \simeq \varepsilon|\gamma|$ and $v_{jn} \simeq \varepsilon\, k|\gamma|$, $R_j$ and $R_e$ are the internal and the external radii of the shear layer, and $Z(z) = z^2 - 2\,C_2 z - \sum_{n=1}^{\infty} A_n\, J_3(\sigma_n)\,[\exp(-\sigma_n z) - 1]$ (where $\sigma_n$ are zeros of $J_2$ and $A_n$ and $C_2$ are constants).

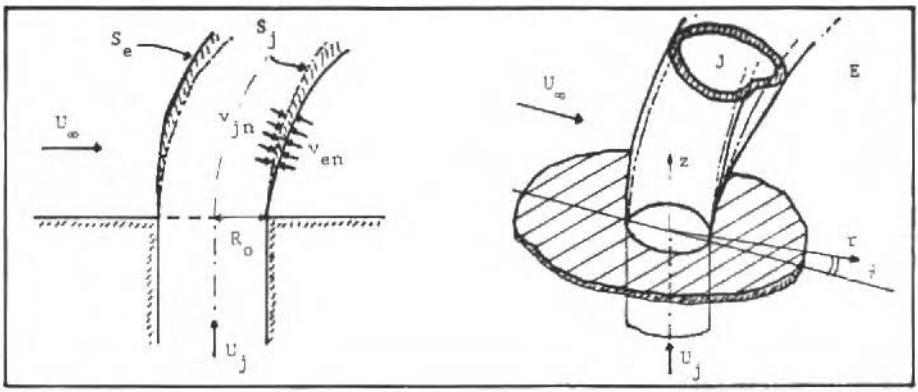


Figure 5. Nomenclature for the entraining vortex-sheet model.

The mean radius $R = (R_e + R_j)/2$ is then:

$$R(\theta, z) = 1 + z\varepsilon + [(1+k)^2\, z^2 \cos\theta]\,\lambda\varepsilon - [Z(z)\cos 2\theta]\,\lambda^2 + O(\lambda^3, \varepsilon^2, \lambda^2\varepsilon) \quad (8)$$

Figure 6 shows the distortion of a initiality planar ring of fluid in the bounding shear layer according to the entraining vortex-sheet model.

General aspects of the topology of the flow along transversal planes are shown in Figure 7. The pattern and the topology of these streamlines is quite different from that of the flow past a rigid bluff body. Firgure 7a shows a single node at the downwind side of the jet contour in the near field. As the jet develops, two nodes appear on the downwind face, where vortices begin to roll up. The number of nodes and saddles satisfy the topological rules set out by [6]. The position of the rear "stagnation" point is a function of $\lambda/\varepsilon$, which is shown

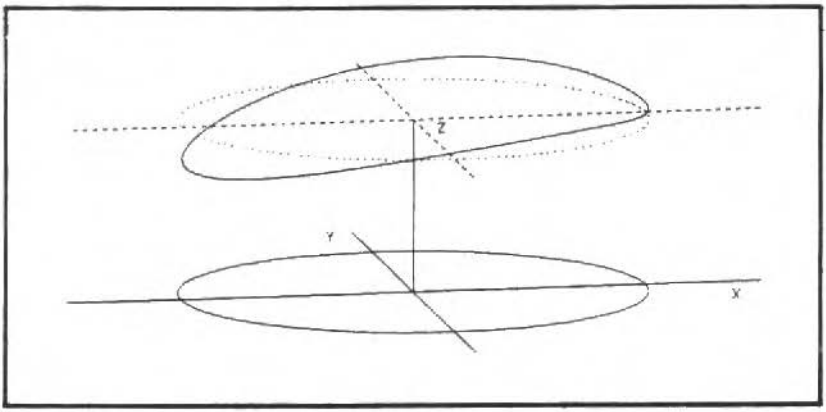


Figure 6. Trajectory of a initially planar ring of fluid in the boundind shear layer, according to the entraining vortex-sheet model. The downwind side of the ring moves faster because of the larger longitudinal velocity induced by the concentration of transversal vorticity in this region.

graphically in Figure 8. This variation of the location of the rear stagnation point is similar to that obtained by the familiar calculation of a line source in a cross-flow [39].

An important aspect of the asymptotic solutions for the entraining vortex-sheet model is the dependence of the initial distortion of the jet on the intensity of the turbulence present in the mixing layer. Different turbulence intensities for the incoming jet flow could induce different turbulent intensities in the mixing layer, determining different entrainment coefficients. The initial distortion of the jet would than be also a function of the level of turbulence present in the incoming flow. However, the intensity of turbulence in the mixing layer is very high ([12] report measurements for $(\bar{u^2})^{1/2}/U_j$ up to .3 in the mixing layer) and so only high levels of turbulence in the incoming jet flow are likely to have sensible effects on the initial developoing of the flow. Turbulence in the oncoming cross-flow is unlikely to have considerable effects on the entrainment coefficient for strong jets because even relatively high turbulence intensities with respect to $U_\infty$ would be negligible with respect to the jet velocity $U_j$, meaning that velocity fluctuations induced by turbulence in the cross-flow are

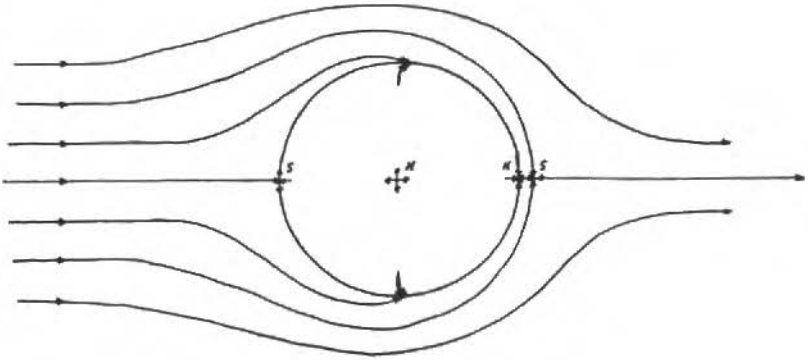


Figure (a)

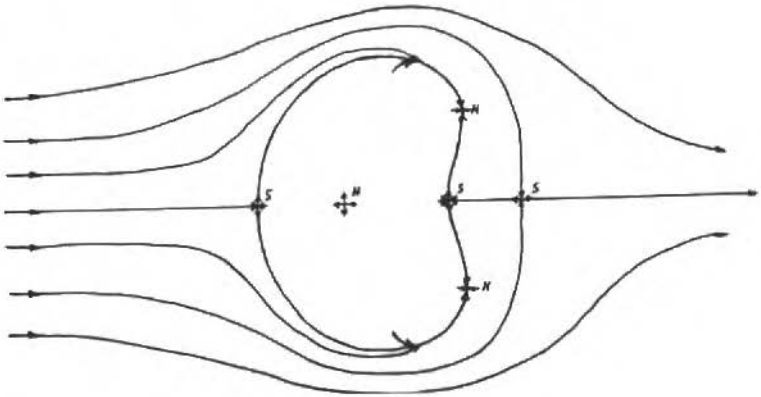


Figure (b)

Figure 7. Topology of the flow over transversal planes: $S$ denotes saddle points and $N$ denotes node points. Figure (a) referes to the initial region only; after the formation of the trailing vortices the topology should be more like figure (b).

very unlikely to be of the same order of magnitude as the velocity fluctuations in the mixing layer. Unfortunately, no systematic measurements of these effects have been found in the literature.

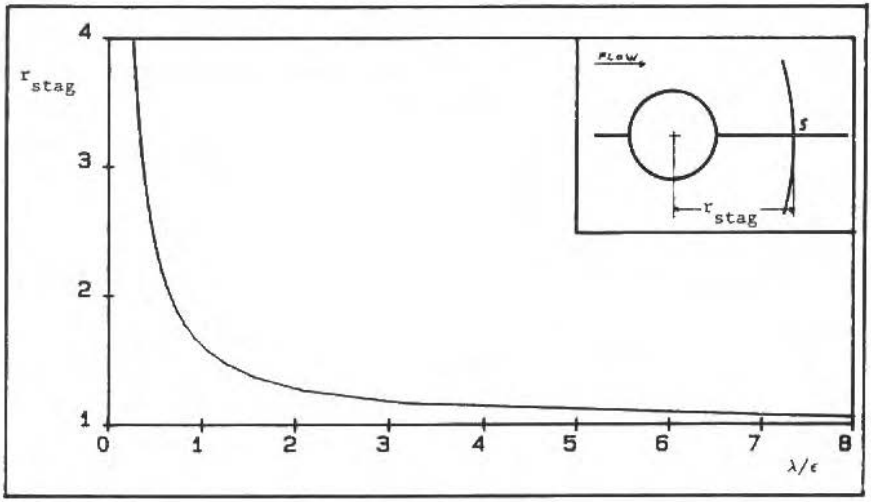


Figure 8. Position of the rear saddle as a function of $\lambda/\epsilon$ (jet stiffness / entrainment coefficient) according to the entraining vortex-sheet model.

Another important result of the entraining vortex-shee model is the prediction of the initial trajectory of the jet. According to expression (8) the position of the centroid of the cross-sections in the initial region is proportional to $\lambda$ and $z^2$ (at the lowest order), leading to $z \propto \lambda^{-1/2}\, x^{1/2}$ (where $x$ is the distance downstream from the jet exit); quite different from the behaviour in the far field. The assumption that the rolled up vortices controle the far field leads to [42] $z \propto \lambda^{-2/3} x^{1/3}$. Experimental researchers seem to find $z \propto \lambda^{-a} x^{b}$, with $a$ varying from .66 to 1 and $b$ from .33 to .39 [3]. The reason for such a wide range of values for these coefficients is probably the fact that the evaluation of these constants is usually based on measurements taken from the whole range of the trajectory of the jet, disregarding the different behaviors suggested by the present result for the initial and far regions. Thus, different ranges at which data is collected determine different values for these constants.

## FINAL REMARKS

The analysis of the mathematical models for jets in cross-flows reported here show, that many of the several models which have been used to describe these

flows are based on completely different explanations of the mechanics of the latter. Recent analytical approach indicates that, at least in the near field of these flows, the effects of turbulent entrainment and the transport of the transversal component of vorticity on the dynamics of the bounding shear layer cannot be neglected. In fact, the effects of pressure drag on the initial distortion of a strong jet in a cross-flow are negligible when compared to the effects of turbulent entrainment.

This transport of transverse vorticity affects the distribuition of the vertical velocity component of the jet: the changes in the vertical velocity distribution induced by this mechanism feed back into the vorticity distribution because it affects the rates at which vorticity vectors are titled, transfering vorticity from one direction to another (see [40]). This process leads to a symmetrical deformation of the bounding vortex-sheet in the inviscid model. A co-flowing component in the external velocity field does brake the symetric of this theoretical flow, but it obviously does not explain the deflection or the distortion of the jet, except when the co-flowing component is large as compared to the cross-flowing component (this case is analysed in [41] and also in [40]).

Therefore, inviscid processes alone are not capable of describing all the features observed in the near field of these flows.

The main effect of viscosity is to generate a shear layer in the boundary of the jet (besides, inviscid vortex-sheets are unstable to all perturbartion modes – see [42]). This shear layer entrains fluid from the external flow, acting theoretically as a sheet of sinks.

In addition to this, the reduced transverse velocity component of the fluid within the inner portions of the shear layer cannot co-exist with an external potential flow along the lee side of the jet. The adverse pressure gradients of this theoretical flow induce the separation of the external portions of this shear layer, and the real flow shows a turbulent wake behing the jet (indeed, a "Von-Karman vortex-street" can be visualized in the wake of the jet – see [40]).

The external flow is therefore similar to the external flow past a bluff body *with surface suction.*

This picture of the flow leads to two main mechanisms for the initial deflection and distortion of the jet: (i) a "pressure-drag" mechanism, due to an asymmetric external pressure distribution (there is a turbulent wake at the lee side of the jet); (ii) an entrainment mechanism, that increases the transverse component of the momentum flux of the jet by adding to the latter the transverse momentum of the entrained fluid.

Either both or one of these mechanisms have been taken into account in the various integral models for jets in cross-flows published in the literature. However, their relative importance to the deflection and distortion of the jet have not been yet properly analysed.

The results reported in [40] show that for velocity ratios $\alpha \simeq 10$ the entrainment mechanism is dominant, and the effects of the asymmetric pressure field are neglible. This dominance of the entrainment mechanism over the pressure-drag mechanism is observed in all jets with $\alpha > 4$, where no deflection of the potential core has been observed. Stronger jets have larger entraining velocities, leading to a stronger suction action on the external flow. Since suction retards the separation of the shear layer, stronger jets have narrower waker, and, consequently, the effects of the pressure-drag mechanism on them are of less importance.

Flows with $\alpha < 4$ have a different picture. In these, the external pressure field induces a sensible drag on the jet and a shift of the potential core in the direction of the stream is observed. The wider wake of these flows have considerable effects on the deformation of the cross-section of the jet.

From the engineering viewpoint, any of the existing integral models do provide satisfactory descriptions for the trajectory and overall size of the jet, within specified ranges of their trajectories. However, these models have been "tuned" for given configurations of the flow (the form of the entrainment function is arbitrality prescribed, and the "tunning" constants are determined by fitting the theory to limited experimental data). They cannot be applied to different configurations of these flows without previous "re-tunning" (modifications of the arbitrary entrainments functions and new coefficients are necessary).

In addition to this, these integral models do not describe either the shape of the jet or the development of the trailing vortex-pair. The evaluation of the

circulation of these vortices would be necessary in improved models for these flows, where the far field would be modeled with the vortex-pair approach. This approach for the far field describes in greater detail the form of the jet and the velocity and concentration distribution, but cannot be applied to the bending over region.

A numerical computation of the flow that would link the "initial conditions" at the near field, as given by the mathematical model developed in chapter 3, to the vortex-pair solution in the far field, might be a consistent way of evaluating the integral parameters and functions to be used in specific integral models for different configurations of the flow. Such integral models would certainly be quite useful in engineering applications.

Even for specific configurations where the far field cannot be described by the free vortex-pair approach (for instance, a jet issuing into a cross-flow in a confined channel), it would still be much simpler to determine a simplified model for the far field of the flow, and connect the near field solution to the far field solution by a numerical computation of the "intermediate field".

The analysis presented in [40] shows that these numerical computations of the flow field of jets as they travel away from the source must consider the effects of turbulent entrainment and the transport of the transverse component of vorticity. The solutions obtained for the intermediate field different configurations of the flow would lead to a better understanding of the physical mechanisms involved in each of these particular configurations.

## REFERENCES

[1] PAI, S. Fluid Dynamics of Jets, D. Van Nostrand Co. Inc., 1954

[2] ABRAMOVICH, G.N. The Theory of Turbulent Jets, MIT Press, 1963

[3] RAJARATNAM, N. Turbulent Jets, Dev. In: Water Sci. - 5, Elsev. Sci. Pub., 1976

[4] KEFFER, J.F. and BAINES, W.D. J. Fluid Mech., vol. 15, pp. 481–496, 1963

[5] COELHO, S.L.V. and HUNT, J.C.R. J. Fluid Mech., vol.200, pp. 95–200, 1989

[6] FOSS, J.F. Report SFB 80/E/161, Univ. Karlsruhe, 1980

[7] HUNT, J.C.R.; ABELL, C.J.; PETERKA, J.A.; WOO, H. JFM, vol. 86, pp. 179–200, 1978

[8] CALLAGHAN, E.E. and RUGGERI, R.S. NACA TN No. 1615, 1948

[9] JORDINSON, R. Aer. Res. Con., R & M n°3074, 1958

[10] KAMOTANI, Y. and GREBER, I., AIAA Journal, 10-11, pp. 1425–1429, 1972

[11] ANDREOPOULOS, J. J. Fluids Eng., vol. 104, pp. 493–174, 1982

[12] ANDREOPOULOS, J. and RODI, W. J. Fluid Mech., vol. 138, pp. 93–127, 1984

[13] ANDREOPOULOS, J. J. Fluid Mech., vol. 157, pp. 163–197, 1985

[14] FEARN, R. and WESTON, R.P. NASA TN D-7916, 1975

[15] THOMPSON, A.M. Ph. D., Thesis, Univ. of London, 1971

[16] MOUSSA, Z.M.; TRISCHKA, J.W.; ESKINAZI, S. J. Fluid. Mech., vol. 80, pp. 49–80, 1977

[17] McMAHON, H.M.; HESTER, D.D.; PALFERY, J.G. J. Fluid Mech., vol. 48, pp. 73–80, 1971

[18] PANKHURST, R.C.; THWAITES, B.; WALKER, W.S. Aer. Res. Con., R & M n° 2787, 1953

[19] HOERNER, S.F. Fluid Dynamic Drag, publ. by the author, pp. 3.1–3.28 , 1965

[20] PLATTEN, J.L. and KEFFER, J.F. Report TP 6808, Univ. of Toronto, 1968

[21] ENDO, H. Trans. Jap. Soc. Aero. Space Sci., vol. 17, n° 36, pp. 45–64, 1974

[22] SUCEC, J. and BOWLEY, W.W., J. Fluids Eng., vol. 98, pp. 667–673, 1976

[23] BRAUN, G.W. and McALLISTER, J.D. NASA SP-218, 1969

[24] MAKIHATA, T. and MIYAI, Y. J. Fluids Eng., vol. 101, pp. 217–223, 1979

[25] SCHATZMANN, M. Atmos. Envir., vol. 13, pp. 721–731, 1978

[26] BATCHELOR, G.K. An Introduction to Fluid Mechanics, Camb. Univ. Press, 1983

[27] ADLER, D.; BARON, A. AIAA Journal, 17–2, pp. 168–174, 1979

[28] CHANG-LU, H. Doctoral Thesis, Univ. Goettingen, 1942

[29] PRATTE, B.D. and BAINES, W.D. J. Hydr. Dvi. – ASCE, HY6, pp. 53–64, 1967

[30] RAJARATNAM, N. and GANGADHARAIAH, T. J. Wind Eng. Ind. Aer., vol.9, pp. 251–255, 1982

[31] DURANDO, N.A. AIAA Journal, vol. 9, nº 2, pp. 325–327, 1971

[32] BROADWELL, J.E. and BREIDENTHAL, R.E. J. Fluid Mech., vol. 148, pp. 405–412, 1984

[33] KARAGOZIAN, A.R. and GREBER, I. AIAA 17th Fluid Dyn. Plas. Dyn. Las. Conf., 1984

[34] SYKES, R.I.; LEWELLEN, W.S.; PARKER, S.F. J. Fluid Mech., 168, pp. 393–413, 1986

[35] FEARN, R. and WESTON, R.P. AIAA Journal, 12–12, pp. 1666-1671, 1974

[36] MARGASON, R.J. NASA SP-218, 1969

[37] HACKETT, J.E. and MILLER, H.R. NASA SP-218, 1969

[38] TAYLOR, G.I. Jour. Aero. Space Sci., vol. 25, pp. 464–465, 1958

[39] MILNE-THOMSON, L.M. Theoretical Hydrodynamics, 4th ed., MacMillan Co., 1938

[40] COELHO, S.L.V. Ph.D. Thesis, Univ. of Cambridge, 1988

[41] NEEDHAM, D.J.; RILEY, N.; SMITH, J.H.B., J. Fluid Mech., 188, pp. 159–184, 1988

[42] DRAZIN, P.G. and REID, W.H., Hydrodynamic Stability, Camb. Univ. Press, 1981

## NOTA OBITUÁRIA

O presente trabalho foi escrito pelo Professor Sérgio L.V. Coelho em seus últimos meses de vida quando os efeitos mais devastadores de sua doença já se manifestavam. Sua carreira curta, mas pontilhada de criatividade e sucesso, foi apenas interrompida em seus últimos dias. Uma opinião abalizada de suas qualidades é emitida a seguir pelo seu antigo orientador de Doutorado na Universidade de Cambridge, Professor J.C.R. Hunt:

"Sergio was an excellent research student who developed every idea or hint that I gave him and often taught me many things in vigorous discussions and arguments! He even took up experimental work which was very unfamiliar to him, and the made a great success of that too! His paper in J.F.M. has already attracted a good deal of attention and has shown some earlier work by the Royal Aircraft Establishment to be incorrect. They are now revising their opinion!"

Prof. A.P. Silva Freire (COPPE/UFRJ)

RBCM – J. of the Braz.Soc.Mech.Sc.
*Vol.XII – nº 3 – pp. 253-270 – 1990*

ISSN 0100-7386
Impresso no Brasil

# CÁLCULO APROXIMADO DE LAS PERDIDAS DE CALOR EN CONDUCTOS HORIZONTALES SUMERGIDOS EN MEDIOS POROSOS COMPLETAMENTE SATURADOS

## *HEAT TRANSFER LOSSES FROM HORIZONTAL DUCTS EMBEDDED IN A SATURED POROUS MEDIUM*

**Ulises Lacoa**
Departamento de Termodinámica
Universidad Simón Bolivar
Caracas 1080-A, Venezuela

**Antonio Campo**
School of Mechanical Engineering
Purdue University
West Lafayette, IN 47907, USA

### RESUMEN

*En este trabajo se presenta un procedimiento de cálculo rápido para la determinación de las distribuciones de la temperatura volumétrica media y de la temperatura de la pared en oleoductos sumergidos horizontalmente en um medio poroso completamente saturado. Los parámetros participantes en el problema combinado de convección son los siguientes: el número de Darcy-Rayleigh, la relación de conductividades, la profundidad adimensional y la posición axial adimensional. La metodologia empleada para resolver el problema descansa sobre la técnica sencilla de formulación concentrada, permitiendo que los cálculos puedan ser realizados con uma calculadora de bolsillo. Los resultados que arroja esta investigación son de gran ayuda para los proyectistas de oleoductos en la industria petrolera, ya que mediante esta metodologia extremadamente simple se podrán determinar la profundidades óptimas con el objeto de minimizar las pérdidas de calor en los oleoductos.*

**Palavras-chave**: Convección Natural en Medio Poroso ▪ Pérdidas de Calor en Oleoductos

### ABSTRACT

*A methodology is presented to allow a quick determination of the average bulk temperature and wall surface temperature of horizontal ducts burried in a saturated porous medium. The governing parameters of the problem are: the Darcy-Rayleigh number, the ratio between the effective thermal conductivity of the medium and the thermal conductivity of the fluid inside the duct, the duct dimensionless depth, and the dimensionless axial location along the duct. For the solution, use is made of a lumped formulation which allows the calculations to be performed using a pocket calculator. The results presented here are of great interest for oleoduct designers in the petroleum industry. Through the simple procedure described herein it is possible to determine optimum depths with respect to heat losses from oleoducts.*

**Keywords**: Natural Convection in Porous Medium ▪ Oleoduct Design

Submetido em Julho/90 Aceito em Agosto/90

## NOMENCLATURA

### Letras Romanas

| | |
|---|---|
| $c_{pi}$ | Calor específico del fluido interno |
| $D$ | Diámetro del tubo |
| $g$ | Aceleración de la gravedad |
| $h_i$ | Coeficiente de convección interno |
| $h_0$ | Coeficiente de convección externo |
| $H$ | Profundidad del eje del tubo |
| $k_i$ | Conductividad térmica del fluido interno |
| $k_0$ | Conductividad térmica del medio poroso externo |
| $K_r$ | Relación de conductividades, $k_0/k_i$ |
| $m$ | Profundidad adimensional del eje del tubo, $H/R$ |
| $\dot{m}$ | Flujo másico |
| $\overline{Nu}_{ef}$ | Número de Nusselt efectivo promedio, $UD/k_f$ |
| $\overline{Nu}_i$ | Número de Nusselt interno promedio, $h_i\ D/k_f$ |
| $\overline{Nu}_0$ | Número de Nusselt externo promedio, $h_0\ D/k_0$ |
| $Q_T$ | Calor total transmitido, ec. (7) |
| $Q_{\max}$ | Calor máximo que puede transmitirse |
| $R$ | Radio del tubo |
| $Ra_w$ | Número de Darcy-Rayleigh basado en la temperatura superficial del tubo, ec. (11c) |
| $Ra_e$ | Número de Darcy-Rayleigh basado en la temperatura de entrada del fluido, ec. (12) |
| $Re_i$ | Número de Reynolds del fluido interno, $u_m D/\nu_i$ |
| $Pr_i$ | Número de Prandtl del fluido interno, $\nu_i/\alpha_i$ |
| $T$ | Temperatura |
| $\bar{U}$ | Coeficiente global de transmisión de calor |
| $u_m$ | Velocidad media del fluido interno |
| $x$ | Variable axial |
| $Z$ | Variable axial adimensional, $x/Re_iPr_i$ |

### Letras Griegras

| | |
|---|---|
| $\alpha_0$ | Difusividad térmica del medio poroso |
| $\beta_0$ | Coeficiente de expansión térmica |
| $\lambda_0$ | Permeabilidad del medio poroso |
| $\alpha_{eq}$ | Difusividad térmica equivalente del medio poroso |

$\theta$ Temperatura adimensional, $(T - T_s)/(T_e - T_s)$
$\rho_i$ Densidad del fluido interno
$\nu_i$ Viscosidad cinemática del fluido interno
$\nu_0$ Viscosidad cinemática del medio poroso externo

**Subíndices**

$b$ volumétrica media
cond conducctión
$e$ entrada
$i$ fluido interno
$o$ medio poroso externo
$s$ interfase entre el medio poroso y el aire
$x$ local
$w$ pared

## INTRODUCTION

La cuantificación de las pérdidas de calor en oleoductos subterráneos constituye un tema de vital importancia en la industria petrolera mundial. Este tema cobra vigencia en el análisis y diseño de oleoductos que transportan crudos pesados e altas temperaturas con el objeto de disminuir la viscosidad de éstos y en consecuencia reducir los costos de bombeo. Igualmente, dentro de un marco ecológico, es importante poder predecir la temperatura en la pared del oeoducto para así conocer el impacto que tendrá el transporte de dicho crudo sobre el medio circundante. Otra aplicación de este tipo de problema se encuentra en las redes de distribución de vapor en las grandes ciudades.

In análise exhaustivo de la literatura especializada refleja que los modelos existentes para determinar la transmisión de calor entre la superficie de un conducto y la superficie de la tierra descansan sobre una hipótesis de conducción de calor bidimensional en el seno de la tierra [1-5]. Sin embargo, en muchas circunstancias, la tierra donde se encuentra sumergida la tubería se torna en um medio poroso permeable al movimiento del agua allí acumulada como producto de las lluvias. En este orden de ideas, la diferencia de temperatura entre el fluido que circula a alta temperatura por la tubería y la superficie libre de la tierra (interfase tierra-aire) induce corrientes de convección natural pura

en la tierra mojada. Aún más, el rol que juega la convección natural en el proceso de transmisión de calor a través de la tierra es tan importante como el causado por la conducción pura. En este sentido, se destaca el estudio pionero de Bau [6], quién obtuvo una solución combinada analítico-numérica para predecir el proceso de convección natural bidimensional en un medio poroso que está entre la superficie de un cilindro sólido y la superficie de la tierra. Esta solución se concibió suponiendo la tierra como un medio poroso saturado caracterizado por un modelo Darciano. Una revisión bibliográfica refleja que existen otros trabajos relacionados a convección natural en medios porosos alrededor de cilindros solidos [7-9]. Sin embargo, éstos consideran el medio poroso de extensión infinita y por lo tanto no se ajustan a los requerimientos de esta investigación.

Con el propósito de enmarcar el problema del transporte de fluidos por conductos subterráneos en un cuadro realista, este trabajo examinará el flujo de un fluido ($Pr \geq 0.7$) a través de una tubería horizontal enterrada en un medio poroso saturado. El calor se libera por convección natural desde la superfície externa del tubo hacia la tierra que la rodea y desde ésta al medio ambiente, que en realidad es el sumidero final. Bajo estas condiciones de operación, la temperatura del fluido interno es superior a la de la superficie de la tierra y las temperaturas volumétrica media del fluido interno y superficial del tubo tenderán a descender en la dirección axial del flujo. Debido a que la convección natural en el medio poroso (la tierra) está controlada por la temperatura local de la superficie del tubo, el coeficiente de convección externa también disminuirá en la dirección del flujo. Esto trae como consecuencia que la variación de la temperatura superficial del tubo se desconozca a priori y que sea producto de la interacción entre los procesos de convección forzada interna en el tubo y de convección natural externa en el medio poroso.

Dentro de esta perspectiva general, el objetivo de esta investigación consiste en determinar aproximadamente la variación axial de la temperatura volumétrica media de un fluido que se transporta por un conducto enterrado en un medio poroso completamente saturado. Conviene señalar que a pesar de la importancia que reviste este problema, los autores no han encontrado trabajos publicados sobre este tema en la literatura especializada.

La técnica de solución para resolver el problema así planteado descansa sobre la hipótesis de una formulación concentrada. Esta formulación ha sido utilizada exitosamente en problemas relacionados al transporte de fluidos en conductos aéreos colocados en posición horizontal o vertical [10,11]. La ventaja máxima que de ella se deriva es que los cálculos son algebráicos y se pueden realizar con una calculadora de bolsillo. De más está decir que esta característica singular la hace extremadamente atractiva para su aplicación práctica en problemas de transporte de crudos y vapor a altas temperaturas.

## FORMULACION MATEMATICA

Considérese un fluido que se transporta con movimiento laminar por una tubería horizontal de radio $R$ enterrada a una profundidad $H$, tal como se muestra en la Fig. 1 anexa. El eje de las tubería coincide con la coordenada axial $x$ y $H$ se mide desde la superficie libre de la tierra, la cual se considera como un medio poroso. En $x = 0$, el perfil de velocidad se encuentra plenamente desarrollado mientras que la temperatura de entrada $T_e$ se supone uniforme. Además, la superficie de la interfase entre el medio poroso semi-infinito y el aire se conserva a una temperatura uniforme $T_s$. El pontencial térmico ($T_e \neq T_s$) induce las corrientes convectivas naturales entre la superficie del tubo y la superficie de la interfase tierra-aire para la región corriente abajo, $x > 0$.

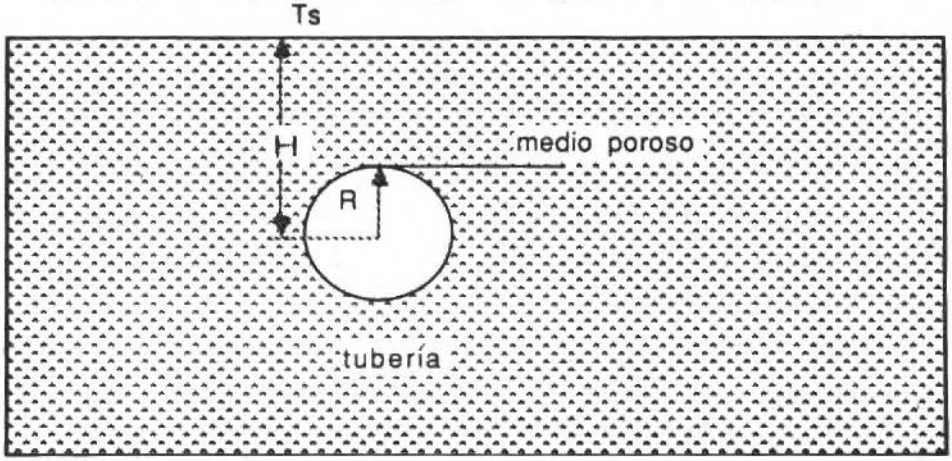


Figure 1. Sistema físico mostrando el tubo sumergido.

Para condiciones de operación estacionarias, el balance de energia sobre el volumen de control dibujado en la Fig. 2 estabelece que

$$(\rho c_p)_i u_m \, dT_b/dx = \pi \dot{D} \, \bar{U}(T_b - T_s) \tag{1a}$$

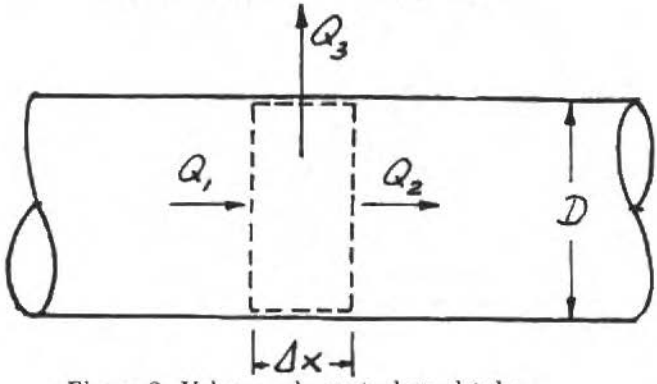


Figure 2. Volumen de control en el tubo.

Esta ecuación diferencial oridnaria está sujeta a la condición de contorno

$$T_b = T_e \quad , \quad x = 0 \tag{1b}$$

En la ec.(1a), el término responsable de las pérdidas de calor lo constituye el coeficiente global de transferencia de calor $\bar{U}$:

$$\bar{U} = (1\bar{h}_i + 1/\bar{h}_0)^{-1} \tag{2}$$

el cual incluye la contribución de todos los mecanismos de transmisión de calor, que actuando en serie, conectan la temperatura volumétrica media del fluido interno $T_b$ con la temperatura de la superficie libre de la tierra $T_s$.

Con el deseo de darle más generalidade a la solución, se propone introducir las variables adimensionales:

$$\theta_b = (T_b - T_s)/(T_e - T_s), \qquad Z = x/(R \; Re_i \; Pr_i)$$

de manera que la ec. (1a) se convierte en

$$d\theta_b/dZ = -2 \, \overline{Nu}_{cf} \, \theta_b \tag{3}$$

En este sentido, integrando la ecuación anterior condicionada a $\theta_b = 1$, $Z = 0$ se tiene la variación de la temperatura volumétrica media del fluido interno. Esto es

$$\theta_b = \exp(-2\overline{Nu}_{ef} Z) \tag{4}$$

en donde el número de Nusselt efectivo promedio está dado por la relación

$$\overline{Nu}_{ef} = \bar{U}\ D/k_i \tag{5a}$$

la cual combinada con la ec. (2) equivale explícitamente a

$$\overline{Nu}_{ef} = \{1/\overline{Nu}_i + 1/[\overline{Nu}_0(k_0/k_i)]\}^{-1} \tag{5b}$$

En la ecuacion anterior, $k_0$ designa la conductividad efectiva del medio poroso y $k_i$ define la conductividad del fluido interno. Por otro lado, el número de Nusselt promedio externo $\overline{Nu}_0$ representa la convección natural en el medio poroso y el número interno $\overline{Nu}_i$ está associado a la convección forzada.

Una vez calculada la temperatura volumétrica media $\theta_b$ empleando la ec.(4), la temperatura de la pared de la tuberia $\theta_w$ puede determinarse mediante la siguiente expresión:

$$\theta_w = \theta_b(1 - \overline{Nu}_{ef}/\overline{Nu}_i) \tag{6}$$

Dentro de este panorama relacionado a la formulación concentrada, conviene destacar que el paso crucial para arribar a la ec. (4) lo constituye la adopción del valor promedio del coeficiente convectivo interno $\bar{h}_i$ o su equivalente el valor promedio del número de Nusselt interno $\overline{Nu}_i$.

### Predicción del calor total liberado

La determinación del calor total $Q_T$ que libera el fluido interno al medio poroso circundante en un tramo de tuberia $x = L$ puede hallarse directamente en virtud del Primer Principio de la Termodinámica. Esto es, usando la relación

$$Q_T = \dot{m} c_{pi}(T_e - T_{x=L}) \tag{7}$$

En cambio si introducimos un valor de referencia $Q_{\max}$, definido como el calor que libera una tuberia con características similares, pero de largo ilimitado, se puede formar el cociente $\Omega$:

$$\Omega = Q_T/Q_{\max} \tag{8a}$$

En realidad, este cociente proporciona una especie de eficiencia térmica, o sea

$$\Omega = (T_{bL} - T_w)/(T_e - T_w) = 1 - \theta_{bL} \tag{8b}$$

que sirve para caracterizar el proceso de transmisión de calor entre el fluido que se transporta por el conducto, el medio poroso (la tierra) y finalmente el aire circundante.

Una ventaja sin paralelo que ofrece esta representación matemática es que con tan sólo una curva de $\theta_b$ vs. $Z$ se puede calcular directamente la temperatura volumétrica media en cualquier estación axial $Z$ y tambien el calor total liberado desde el origen $Z = 0$ hasta dicha estación $Z$.

## MODELO PARA LA CONVECCION FORZADA INTERNA

La superficie del volumen de control dibujado en la Fig. 2 se supone que está en equilibrio isotérmico. Por lo tanto, en lo concerniente al proceso de convección forzada interna, la expresión apropiada para el número de Nusselt promedio $\overline{Nu_i}$ viene dada por las correlaciones recomendadas por Shah [12,13] para el caso de régimen laminar en tubos suponiendo una temperatura superficial constante. Estas se desglosan por tramos de la siguiente manera:

$$\overline{Nu_i} = 2.0348\ Z^{1/3} - 0.7, \qquad Z < 0.01 \tag{9a}$$

$$\overline{Nu_i} = 2.0348\ Z^{1/3} - 0.2, \qquad 0.01 < Z < 0.06 \tag{9b}$$

$$\overline{Nu_i} = 3.657 + 0.0998\ Z^{-1}, \qquad Z > 0.06 \tag{9c}$$

## MODELO PARA LA CONVECCION NATURAL EN EL MEDIO POROSO

Se sabe que el número de Nusselt externo $\overline{Nu}_0$ depende tanto de la profundidad $H$ a la cual se encuentra ubicada la tubería, como del número de Darcy-Rayleigh referido a una diferencia de temperatura $\Delta T$:

$$Ra = g\beta_0(\Delta T)\ \lambda_0\ T/\nu_0\ \alpha_{eq} \tag{10}$$

Como en este trabajo se persigue estudiar la convección natural desde la superficie del tubo hasta la superficie de la tierra, $\Delta T$ debe escogerse de acuerdo a los requerimientos de la formulación concentrada adoptada.

En el trabajo clásico de Bau [6] se examino el fenómeno de convección natural en um medio poroso colocado entre un cilindro sólido isotérmico ($T_w$) y una superficie horizontal e isotérmica ($T_s$). El producto de esta investigación, la cual es de carácter bidimensional, arroja la siguiente correlación

$$Nu_0 = NU_{\text{cond}}\left[\frac{1 + 10^{-2}m(1.084\ m^{0.393} - 0.71)\ Ra_w^2}{1 + 0.28m^{0.4}Ra_w}\right] \tag{11a}$$

siendo $m$ la profundidad adimensional y

$$Nu_{\text{cond}} = 2/\ln\left[m + \sqrt{(m^2 - 1)}\right] \tag{11b}$$

la expressión asociada al transporte de calor en un medio puramente conductivo.

Bajo la hipótesis de que el tubo se encuentra en equilibrio isotérmico en cada volumen de control, el problema en estudio se amolda perfectamente a los resultados reportados en [6], pero introduciendo una pequeña variante. Tornando nuestra atención a la estructura de número de Darcy-Rayleigh $Ra_w$, se desprende que éste no es un parámetro constante en el marco del problema. Esto se debe a que $T_w$ se desconoce a priori y depende intimamente de la interacción de los mecanismos de convección natural en el medio poroso y convencción forzada en el flujo interno. Por consiguiente, se puede definir un nuevo número de Darcy-Rayleigh designado por $Ra_e$

$$Ra_e = g\ \beta_0(T_e - T_s)\ \lambda_0\ R/\nu_0\ \alpha_{eq} \tag{12}$$

que involucra la diferencia entre la temperatura de entrada $T_e$ y la temperatura de la superficie libre $T_w$. Es decir, la diferencia de temperatura máxima en el proceso térmico.

En virtud del argumento anterior, $Ra_w$ en la ec. (11a) se puede reemplazar por la relación equivalente

$$Ra_w = Ra_e\ \theta_w^{-1} \tag{13}$$

## PROCEDIMIENTO DE CALCULO

Una inspección de la formulación del problema confirma que su solución está regida por los parámetros adimensionales:

1. El número de Darcy-Rayleigh, $Ra_e$
2. La profundidad adimensional, $m = H/R$
3. La relación de conductividades, $K_r = k_0/k_i$
4. La posición axial adimensional $Z$

En procedimiento de cálculo se describe una vez conocidos estos datos y los pasos a seguir están resumidos a continuación:

1. Se calcula $\overline{Nu_i}$ empleando la correlación apropiada (ver ec. (9))
2. Se propone un valor inicial de $\theta_w^{(0)}$
3. Se calcula $\overline{Nu_0}$ mediante la ec. (11)
4. Se determina $\overline{Nu_{ef}}$ con la ec. (5)
5. Se obtiene $\theta_b^{(0)}$ usando la ec. (4)
6. Se calcula un valor nuevo de $\theta_w$, o sea $\theta_w^{(1)}$ con la ec. (6)

Una vez que se satisface el criterio de convergencia

$$\left|\theta_w^{(i+1)} - \theta_w^{(i)}\right| < 0.001$$

el proceso se detiene. Si esto no ocurre, se toma el valor nuevo de $\theta_w^{(1)}$ y se regresa al punto 2 para proseguir la secuencia hasta que se obtenga la convergencia de $\theta_w$ propuesta.

Conviene señalar que la rapidez de convergencia depende exclusivamente de la buena escogencia del valor inicial de $\theta_w^{(0)}$. A continuación se presenta un ejemplo que ilustra el procedimiento de cálculo.

### Ejemplo de cálculo

Dados los datos:

$$Ra_e = 10,\ m = 2 \quad \text{y} \quad K_r = k_0/k_i = 1$$

se desea calcular: a) la temperatura volumétrica media del fluido y b) la temperatura de la pared del tubo, ambas en la estación $Z = 0.001$.

La secuencia de cálculos correspondiente se resume en la tabla anexa:

| iteración $i$ | $\theta_w^{(i)}$ | $\overline{Nu_0}^{(i)}$ | $\overline{Nu_i}$ | $\overline{Nu_{ef}}^{(i)}$ | $\theta_b^{(i)}$ | $\theta_w^{(i)}$ |
|---|---|---|---|---|---|---|
| 0 | 1 | 1.6631 | 19.648 | 1.5333 | 0.9969 | 0.9220 |
| 1 | 0.9220 | 1.6143 | 19.648 | 1.4917 | 0.9970 | 0.9213 |
| 2 | 0.9213 | 1.6139 | 19.648 | 1.4917 | 0.9970 | 0.9213 |

Como se observa, tan solo tres interaciones son necesarias para obtener el resultado final. Entretanto, si se desean realizar los cálculos para $\theta_b^{(p+1)}$ y $\theta_w^{(p+1)}$ en otras estaciones corriente abajo se puede emplear el valor de $\theta_w$ calculado en la estación anterior como suposición inicial, o sea $\theta_w^{(0)}$.

## PRESENTACION DE LOS RESULTADOS

### Convección natural en el tubo expuesto al aire

Con el propósito de validar los resultados por via de la formulación concentrada con cálculos algebráicos, se presenta primero la comparación para el caso de una tubería aérea expuesta a convección natural. Para ello, se emplean dos casos limites del cociente de conductividades $K_r$, es decir $K_r = 0.05$ (combinación de agua adentro y aire afuera) y $K_r = 20$ (combinación de aire adentro y agua afuera). El patrón de referencia lo constituye los resultados precisos de Faghri y Sparrow [14], quiénes emplearon una formulación diferencial en unión de una solución numérica. En las Figs. 3 y 4 se dibujan las variaciones de la temperatura volumétrica media y de la temperatura superficial del tubo. Aqí puede corroborarse la buena concordancia que existe en toda la gerión de desarrollo térmico usando los dos modelos citados que son totalmente diferentes.

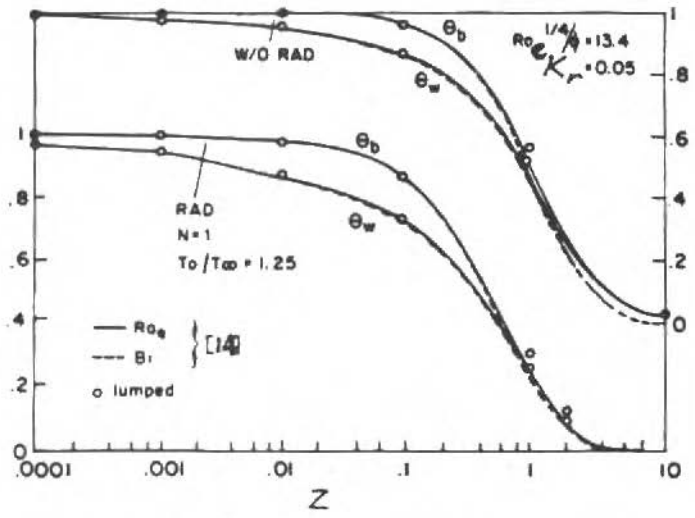


Figure 3. Comparación de las distribuciones de temperatura para un tubo aéreo ($K_r < 1$)

### Convección natural en el tubo expuesto al medio poroso

Los parámetros termogeométricos escogidos son los siguientes: el número de Darcy-Rayleigh $Ra_e = 10$ y 40, la profundidad adimensional $m$ comprendida entre 2 y 8 y las relaciones de conductividades $K_r = 0.1$, 1, y 10.

La discusión de esta situación física comienza con la Fig. 5 en donde $Ra_e = 10$. Para el caso $K_r = 10$, la curva de $\theta_b$ desciende rapidamente para una profundidad $m = 2$. Este comportamiento es de esperarse ya que la tubería está muy cercana a la interfase y la resistencia térmica que brinda el medio poroso es muy baja. A medida que la profundidad adimensional $m$ aumenta ($2 < m < 8$), las curvas $\theta_b$ se desplazan hacia arriba ordenamente. En la subfamilia de curvas puede observarse que la dependencia de $\theta_b$ con $Z$ es la más lenta para una profundidad de $m = 8$. O sea que, desde un punto de vista de conservación de energía en el fluido interno conviene enterrar la tubería lo máximo posible. Esto indica que la resistencia térmica del medio poroso tiende

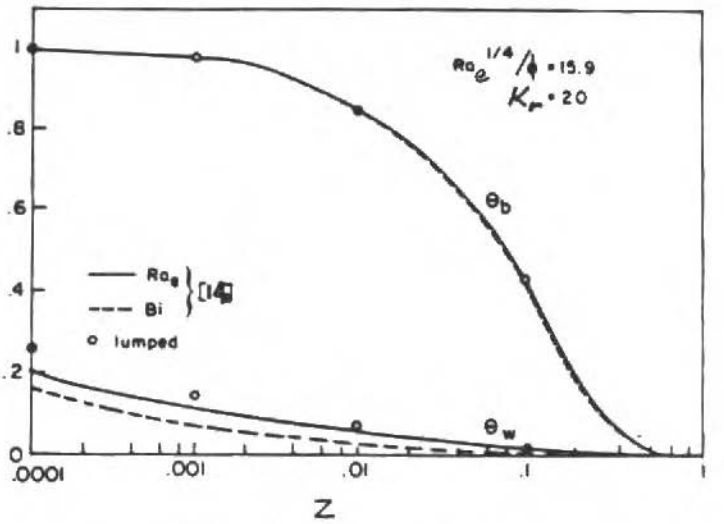


Figure 4. Comparación de las distribuciones de temperatura para un tubo aéreo ($K_r > 1$)

a aumentar, por supuesto con $m$. Además, conviene señalar que la separación $\Delta\theta_b$ entre la curva con $m = 2$ y la curva con $m = 8$ prevalece invariante con la coordenada axial, esto es $\Delta\theta_b = 0.05$ unidades aproximadamente.

El próximo caso a discutir corresponde a $K_r = 1$, o sea el mismo fluido afuera y adentro. Aquí de nuevo, la subfamilia de curvas parametrizadas para $m$ muestra un comportamiento monótono decreciente. La caída más rápida de la temperatura corresponde a $m = 2$ y por el contrario, la más lenta está asociada a $m = 8$. Puede observarse que no existe una diferencia apreciable entre las curvas com $m = 6$ y $m = 8$. Estas serían las profundidades recomendadas para las situaciones en donde se persigue liberar poca energía al medio ambiente. Además, se aprecia un patrón de abanico en donde la desviación máxima $\Delta\theta_b$ tiende a aumentar corriente abajo. Por otro lado, la distancia $\Delta\theta_b$ entre la curva $m = 2$ y la que le sigue $m = 4$ es pronunciada. Esta distancia tiende a disminuir y las curvas tienden a juntarse a medida que $m \geq 4$. Para una

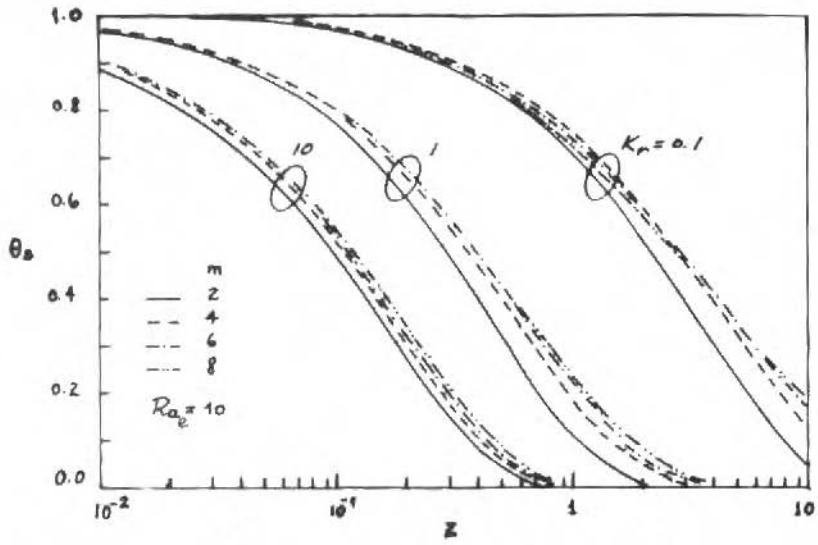


Figure 5. Distribución de la temperatura volumétrica para un tubo sumergido ($Ra_e = 10$)

tubería de longitud $Z = 0.6$, para efectos prácticos, las curvas de $m = 6$ y $m = 8$ coinciden.

El grupo de curvas ralacionadas a $K_r = 0.1$ describen un comportamiento un poco diferente al de los casos anteriores con $K_r = 1$ y 10. Si consideramos una tubería de largo $Z = 2.5$, la caída más lenta de temperatura $\theta_b$ ocurre cuando $m = 4$. El orden de las curvas corresponde a $m = 6$, $m = 8$ y finalmente la variación más rápida tiene lugar a una profundidad de $m = 2$. Este hecho demuestra que para $K_r = 0.1$ existen profundidades óptimas, en donde se pone de manifiesto un efecto compensatorio entre las resistencias térmicas. Cuando $Z > 0.6$, el orden de las curvas se restabelece al igual que en los casos anteriores. También es de notar que el campo térmico se ha desarrollado plenamente para $K_r = 10$ en $Z = 0.8$. Sin embargo, este desarrollo de la temperatura tiende a hacerse cada vez mayor a medida que $K_r$ disminuye, observándose que en $Z = 10$ la temperatura no se ha desarrollado aún para $K_r = 0.1$. Asimismo, la Fig. 6 describe la variación de la temperatura superficial $\theta_w$ asociada a la

Fig. 4. A rasgos generales, la tendencia es acorde a lo explicado anteriormente para $\theta_b$.

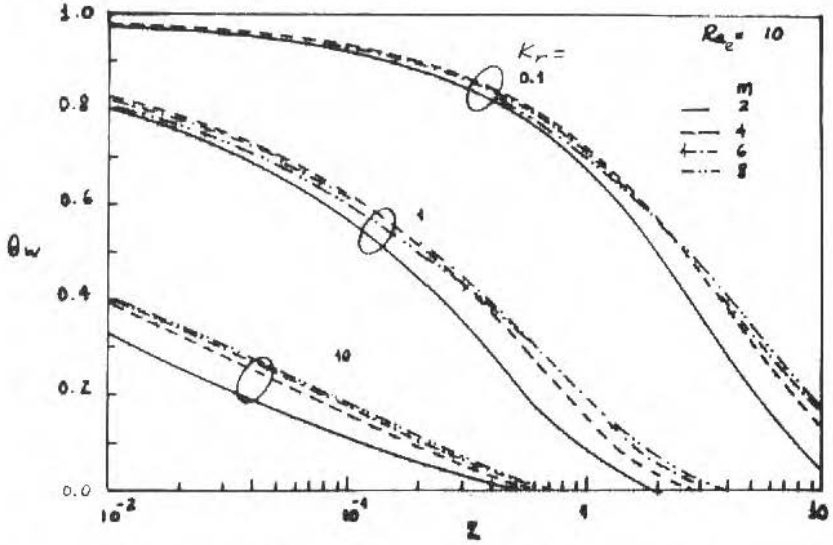


Figure 6. Distribución de la temperatura superficial para un tubo sumergido ($Ra_e = 10$)

El efecto que ejerce el número de Darcy-Rayleigh con valor $Ra_e = 40$ sobre la temperatura volumétrica media se dibuja en las Figs. 7 y 8. Primeramente, para $K_r = 10$ todas las curvas tienden a ser invariantes con $Z$ has $Z = 10^{-1}$. De ahí en adelante el patrón normal prevalece, o sea $\theta_b$ disminuye a medida que $m$ aumenta.

Para $K_r = 1$, el abanico de curvas tiende a abrirse más en función de $m$. Ocurre un cruzamiento de las curvas en $z = 0.3$. Hasta esta estación, $\theta_b$ desciende lentamente para $m = 2$ y rápidamente para $m = 8$. En cambio, cuando $Z > 0.3$, $\theta_b$ cae lentamente para $m = 8$ y rápidamente para $m = 2$. Como es de esperarse, las magnitudes de las resistencias térmicas juegan un papel determinante en este comportamiento.

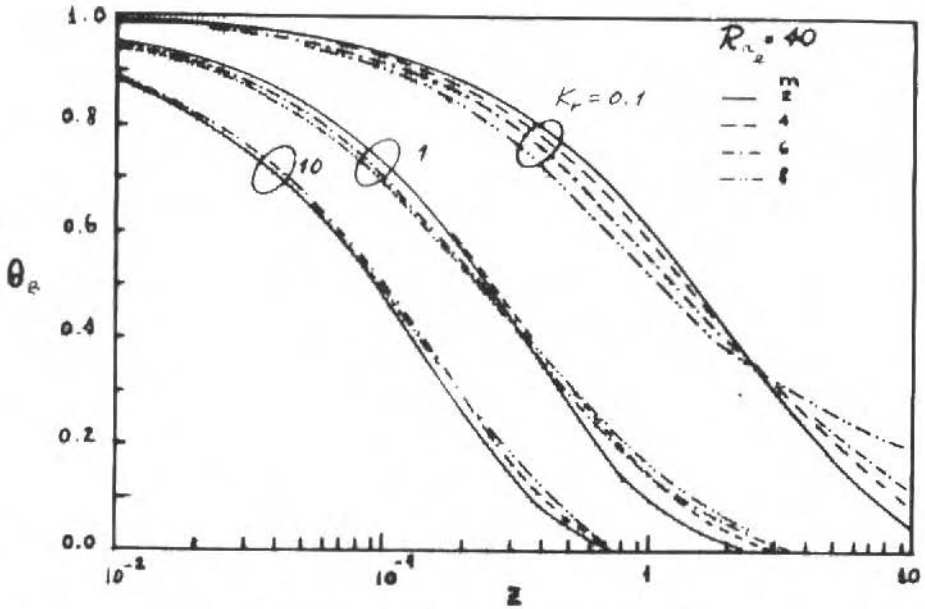


Figure 7. Distribución de la temperatura volumétrica para un tubo sumergido ($Ra_e = 40$)

Finalmente, la subfamilia de curvas governadas por $K_r = 0.1$ muestra un comportamiento análogo al de $K_r = 1$ pero con una dispersión más marcada. El patrón explicado para $K_r = 0.1$ se repite aquí también pero con mayor intensidad, ocurriendo el punto de corte de las curvas en $Z = 2.5$. Este fenómeno ocurre hasta la estación axial $Z = 2.5$, en donde de ahí en adelante el orden de las curvas se invierte. Esta situación anómala se explica, vía las resistencias térmicas características, o sea que la resitencia conductiva domina en la región $Z < 2.5$, en tanto que la resistencia convectiva es preponderante para la región $Z > 2.5$.

De igual manera, las curvas de $\theta_w$ vinculadas a la Fig. 7 se dibujan en la Fig. 8, apreciándose una dependencia con $Ra_e$, $m$, $K_r$, y $Z$ bastante similar a la observada para $\theta_b$ en la Fig. 6.

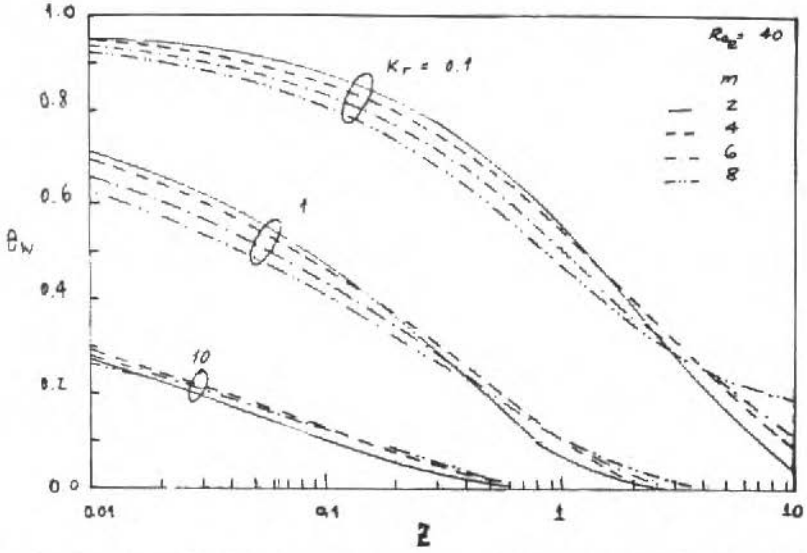


Figure 8. Distribución de la temperatura superficial para un tubo sumergido ($Ra_e = 40$)

## REFERENCES

[1] SCHOFIELD, F.H., The Steady Flow of Heat from Certain Objects Buried under Flat-air-cooled Surfaces, Phil Magazine, vol.31, pp. 471–497, 1941.

[2] ECKERT, E.R.G. & DRAKE, R.M. Analysis of Heat and Mass Transfer, pp. 92–102, McGraw-Hill, N.Y., 1972.

[3] THYAGARAJAN, R. & YOVANOVICH, M. Thermal Resitance of a Buried Cylinder with Constant Flux Boundary, J. Heat Transfer, vol.96, 249–250, 1974.

[4] BAU, H.H. & SADHAL, S.S., Heat Losses from a Fluid in a Buried Pipe, International J. Heat Mass Transfer, vol. 25, 1621–1629, 1982.

[5] SCHNEIDER, G.E. An Investigation of the Heat Losso Characteristics of Buried Pipes, Journal Heat Transfer, vol.107, 696–699, 1985.

[6] BAU, H.H. Convective Heat Losses from a Pipe Buried in a Semi-Infinite Porous Medium, International J. Heat Mass Transfer, vol. 27, 2047–2056, 1984.

[7] SCHROCK, V.E.; FERNANDEZ, R.T. & KESAVAN, K. Heat Transfer from Cylinders Embedded in a Liquid Filled Porous Medium, Proc. International Heat Transfer Conference, Paris, France, Paper CT 3.6, 1970.

[8] FERNANDEZ, R.T. & SCHROCK, V.E. Natural Convection from Cylinders Buried in a Liquid Saturated Porous Medium, Proc. International Heat Transfer Conference, Munich, Federal Republic of Germany, 2, 335–340, 1982.

[9] FAROUK, B. & SHAYER, H. Natural Convection Around a Heated Cylinder Buried in a Saturated Porous Medium, J. Heat Transfer. v.110, 642–650, 1988.

[10] CAMPO, A. & LACOA, U. The Simplest Approach to Forced Convection in Horizontal Pipes Exposed to Natural Convection and Radiation, International Comm. Heat Mass Transfer, vol.14, 551–560, 1987.

[11] CAMPO, A. & LACOA, U. Laminar Forced Convection in Vertical Pipes Exposed to External Natural Convection and External Radiation: Uncoupled / Lumped Solution, Wärme-und Stoffübertragung, vol.25, 1–8, 1989.

[12] SHAH, R.K. Thermal Entry Length Solutions for the Circular Tube and Parallel Plate Channels, Paper no. 11-75, Proc. National Heat and Mass Transfer Conference, Bombay, India, 1975.

[13] SHAH, R.K. & LONDON, A.L. Laminar Flow Forced Convection in Ducts, Academic, New York, 1978.

[14] FAGHRI, M. & SPARROW, E.M. Forced Convection in a Horizontal Pipe Subjected to Nonlinear External Natural Convection and to External Radiation, International J. Heat Mass Transfer, vol.23, 861–871, 1980.

**RBCM – J. of the Braz.Soc.Mech.Sc.** ISSN 0100-7386
*Vol.XII – nº 3 – pp. 271-286 – 1990* Impresso no Brasil

# PETROV-GALERKIN/MODIFIED OPERATOR SOLUTIONS OF STEADY-STATE CONVECTION DOMINATED PROBLEMS

## *UM MÉTODO DE PETROV-GALERKIN/OPERADOR MODIFICADO PARA SOLUÇÃO DE PROBLEMAS ESTACIONÁRIOS COM CONVECÇÃO DOMINANTE*

**P.A.B. de Sampaio**
Dept. of Civil Engineering
University College of Swansea
SA2 8PP U.K.

### ABSTRACT

*A new Petrov-Galerkin method to deal with convection-diffusion problems is presented. The formulation is derived from the concept of using a modifying function to make the differential operator self-adjoint. The so-called 'optimal upwind' parameter ($\alpha$) arises naturally from the process of approximating the modifying function. Applications to steady-state problems in two dimensions are shown.*

**Keywords**: Convection-Diffusion ▪ Petrov-Galerkin Methods ▪ Upwind Techniques

### RESUMO

*Apresenta-se um novo método de Petrov-Galerkin para solução de problemas convectivo-difusivos. A formulação baseia-se no uso de uma função modificadora que torna o operador diferencial auto-adjunto. O chamado parâmetro ótimo de 'upwind' aparece naturalmente no processo de aproximação da função modificadora. Aplicações do método a problemas estacionários em duas dimensões são mostradas.*

**Palavras-chave**: Convecção-Difusão ▪ Métodos de Petrov-Galerkin ▪ Técnicas de 'Upwind'

Submetido em Agosto/89 Aceito em Agosto/90

## INTRODUCTION

It is well known that the use of Galerkin's method to solve strong convective problems produces oscillatory results. The difficulties arise from the non self-adjoint character of the convection-diffusion differential operator, for which the 'best approximation property' of the Galerkin formulation is lost [1]. In the finite element context most of the efforts to solve convection-diffusion problems have used 'upwind' procedures introduced via Petrov-Galerkin methods [2], [3]. Soon it was realised, though, that like their finite difference counterparts, finite element 'upwind' procedures tended to produce overdiffusive solutions in multidimensional and transient situations [4].

A major advance was obtained with the development of the 'Streamline Upwind Petrov-Galerkin' method (SUPG), also known as 'Anisotropic Balancing Dissipation' [4], [5]. In such methods the 'upwinding' is performed only in the streamline direction and hence the amount of numerical diffusion is considerably reduced. Nevertheless, oscillations can occur near sharp layers as the matrices obtained do not keep diagonal dominance in multidimensional cases. The SUPG method has been recently improved with the addition of 'Discontinuity Capturing Terms', though at the expense of a non-linear mechanism, as these extra terms depend on the solution itself [6], [7].

In this paper we concentrate our attention on the steady-state problem. A new Petrov-Galerkin formulation is derived from the concept of using a modifying function to make the differential operator self-adjoint [8], [9], [10]. In fact, the Petrov-Galerkin weightings are determined from approximations of the modifying function. For the one-dimensional case the so-called 'optimal upwind' scheme is obtained without using previous knowledge of the analytical solution. Later in the paper we extend the algorithm in order to deal with two-dimensional problems. A special treatment of the streamline derivative is introduced, which guarantees the diagonal dominance of the resulting equation system. This prevents the occurence of non-physical oscillations and enhances the possibilities of using iterative solvers.

Finally, the performance of the formulation is shown in two-dimensional examples, with special attention being paid to the strong convection case.

## DERIVATION OF THE NEW PETROV-GALERKIN METHOD

It is commented in [1] that 'upwinding' techniques and 'symmetrization' of non self-adjoint problems are related procedures. As we shall see in the following derivation, this concept is directly used to establish a new Petrov-Galerkin method.

Consider the convection-diffusion problem given by the energy equation for an incompressible flow in the one space coordinate $x$:

$$\rho\, c_p u \frac{dT}{dx} - \kappa \frac{d^2T}{dx^2} = Q \tag{1}$$

where:

$\rho$ is the density.
$c_p$ is the specific heat.
$\kappa$ is the thermal conductivity.
$u$ is the flow velocity in the $x$-direction.
$T$ is the temperature.
$Q$ is the volumetric heat source.

The differential operator associated with equation (1) is non self-adjoint due to the presence of the convective terms. The result is that the Galerkin method does not possess the 'best approximation property' for discretising equation (1).

Using an idea presented by Gaymon et al. [8] and also described in Zienkiewicz [12], the differential operator can be made self-adjoint using a suitable multiplying function. Integrating equation (1) over a typical element the following weighted residual statement is obtained:

$$\int_e \phi f \left( \rho\, c_p u \frac{dT}{dx} - \kappa \frac{d^2T}{dx^2} \right) dx = \int_e \phi f\, Q\, dx \tag{2}$$

The diffusive term is integrated by parts to give:

$$\int_e \phi \frac{dT}{dx} \left( \rho\, c_p u f + \kappa \frac{df}{dx} \right) dx + \int_e \kappa f \frac{d\phi}{dx} \frac{dT}{dx}\, dx = \int_e \phi f\, Q\, dx + \text{b.t.} \tag{3}$$

where b.t. represents the heat-flux boundary terms.

We notice that the first term in equation (3) is non-symmetric and that the differential operator is non self-adjoint. Nevertheless, self-adjointness can be recovered by suitably defining $f$, the modifying function. For locally constant velocity and properties the non-symmetric term vanishes if one sets

$$f = C_0 \exp\left( - \frac{\rho c_p u}{\kappa} x \right) \tag{4}$$

In equation (4) the constant $C_0$ is to be determined in such a way that continuity of $f$ is preserved over a typical assembly of elements. For instance, for linear elements and using local non-dimensional coordinates we have (see figure (1)).

$$f_i = C_1 \exp\left[ \frac{P(\xi_i - \xi)}{2} \right] \tag{5}$$

where $P$ is the element Peclet number given by

$$P = \frac{\rho c_p u h}{\kappa} \tag{6}$$

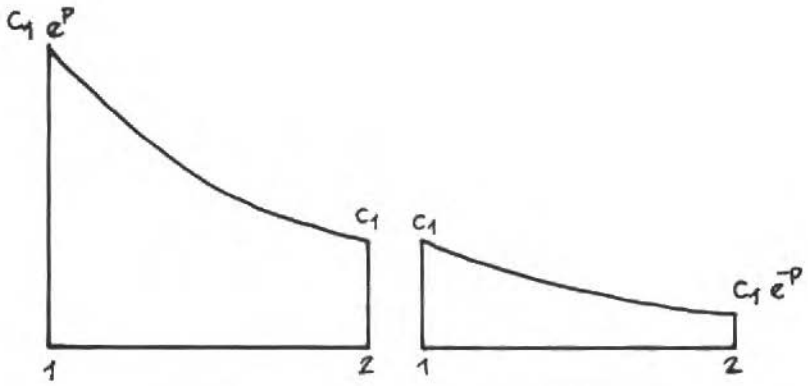


Figure 1. Modifying function over an assembly of linear elements.

The node coordinates for the linear element are:

$$\xi_i = \begin{cases} -1 & \text{for } i = 1 \\ +1 & \text{for } i = 2 \end{cases} \tag{7}$$

$C_1$ is a normalising constant such that

$$C_1 \int_{-1}^{+1} \exp\left(-\frac{P\xi}{2}\right) d\xi = 2 \tag{8}$$

If $L$ is the original differential operator associated with equation (1), we see that the role of the function $f$ is to produce a new operator $L^* = fL$ which is self-adjoint. For that reason we call $f$ the modifying function. Note that with $f$ defined according to equation (5) we are able to deal with variable properties, using local (element) values. On the other hand, the symmetry of the overall equation system is lost as we define different modifying functions for different assemblies.

It is important to note that equation (3) requires continuity of $f$ on the assembly, otherwise the inter-element boundary terms do not cancel. This restriction can be circumvented by returning to equation (2) and splitting $\phi f$ into $\phi$ and $\phi(f-1)$. Now, assuming $\phi$ to be continuous, we can integrate by parts only those diffusive terms which are weighted by $\phi$. This procedure can be interpreted within the framework presented in [11] and it is clear that $f$ does not need to be continuous in this case. The resulting formulation is:

$$\int_e \left(\phi f\, \rho c_p u \frac{dT}{dx} + \kappa \frac{d\phi}{dx}\frac{dT}{dx}\right) dx - \int_e \phi(f-1)\,\kappa \frac{d^2T}{dx^2}\, dx = \int_e \phi f\, Q\, dx + \text{b.t.} \tag{9}$$

Equation (9) allows the use of a piecewise constant approximation of the modifying function. Therefore, restricting our attention to linear elements, the linear shape functions can be used as weightings to determine two different constant approximations for the exponential $C_1 \exp(-P\xi/2)$:

$$\int_{-1}^{+1} N_1[C_1 \exp(-P\xi/2) - A]\, d\xi = 0 \tag{10}$$

$$\int_{-1}^{+1} N_2[C_1 \exp(-P\xi/2) - B]\, d\xi = 0 \tag{11}$$

where

$$N_i = 0.5(1 + \xi_i\xi) \tag{12}$$

From the above equations we obtain

$$A = 1 + \alpha \tag{13}$$

$$B = 1 - \alpha \tag{14}$$

with

$$\alpha = \coth(P/2) - 2/P \tag{15}$$

The piecewise constant modifying functions is defined using these approximation as

$$f_i = 1 + \alpha\xi_i \tag{16}$$

A representation of equation (16) over a typical assembly is shown is figure (2).

It should be noticed that the parameter $\alpha$, given by equation (15), is the so-called 'optimal upwind' parameter adjusted in other Petrov-Galerkin formulations in order to give nodally exact solutions for steady-state problems. Here, though, no previous knowledge of the analytical solution has been used to obtain it.

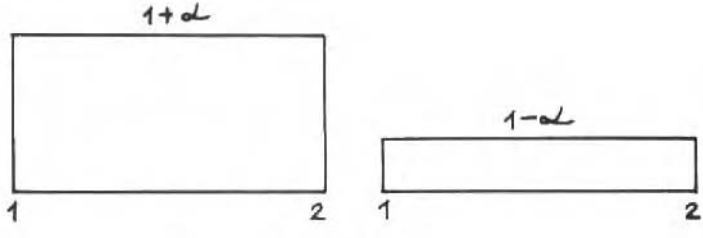


Figure 2. Piecewise constant $f$.

So far we have discussed in some detail how to define $f$, but we have not said much about $\phi$. If we look back into equation (2) we can see that an 'optimal' choice is to have $\phi$ belonging to the same space as $T$ (apart from non-homogeneous essential boundary conditions). In this case we can regard equation (2) as a Galerkin method applied to the modified self-adjoint operator, a procedure known to possess the 'best approximaton property'. Note that equation (2) can be also seen as a Petrov-Galerkin formulation, where the weighting $\phi f$ is applied to the original non self-adjoint problem. It is clear that the procedure becomes the Galerkin method as $P \rightarrow 0$.

For linear elements we obtain the following general equation for an internal node:

$$-\Big[1+\frac{P(1+\alpha)}{2}\Big]\,T_{i-1}+(2+\alpha P)\,T_i-\Big[1-\frac{P(1+\alpha)}{2}\Big]\,T_{i+1}=\frac{Qh^2}{\kappa} \qquad (17)$$

In the above equation diagonal dominance is preserved for the whole range of the Peclet number, Equation (17) is in fact the so-called 'optimal upwind' scheme, giving nodally exact solutions on uniform meshes.

## 2D-PROBLEMS

Two-dimensional problems are considered in this section. The methodology described earlier is extended and bilinear Lagrangian elements are employed in the discretisation.

For two-dimensional flows the weighted residual statement given in equation (2) is replaced by

$$\int_{\Omega_e}\phi f\Big[\rho\,c_p\Big(u\,\frac{\partial T}{\partial x}+v\,\frac{\partial T}{\partial y}\Big)\Big]\,d\Omega-\int_{\Omega_e}\phi f\,\kappa\Big(\frac{\partial^2 T}{\partial y^2}\Big)\,d\Omega=\int_{\Omega_e}\phi f\,Q\,d\Omega \qquad (18)$$

where $u$, $v$ are the velocity components in the $x, y$ directions, respectively.

Following the same arguments presented in section 2, it is a simple matter to check that self-adjointness requires the modifying function to be

$$f = C_0 \exp\Big[-\frac{\rho c_p}{\kappa}(ux + vy)\Big] \tag{19}$$

Returning to equation (18), we split the weghting $\phi f$ into $\phi$ and $\phi(f-1)$. Integrating by parts those diffusive terms which are weighted by $\phi$ we obtain

$$\int_{\Omega_e} \phi f\Big[\rho\, c_p\Big(u\,\frac{\partial T}{\partial x} + v\,\frac{\partial T}{\partial y}\Big)\Big]\, d\Omega + \int_{\Omega_e} \kappa\Big(\frac{\partial \phi}{\phi x}\,\frac{\partial T}{\partial x} + \frac{\partial \phi}{\partial y}\,\frac{\partial T}{\partial y}\Big)\, d\Omega -$$

$$\int_{\Omega_e} \phi(f-1)\,\kappa\Big(\frac{\partial^2 T}{\partial x^2} + \frac{\partial^2 T}{\partial y^2}\Big)\, d\Omega = \int_{\Omega_e} \phi f\; Q\; d\Omega + \text{b.t.} \tag{20}$$

Again, the shape functions can be used as weightings to determine constant approximations for the exponential given in equation (19). The piecewise constant modifying function is given by

$$f_i = (1 + \alpha_\xi \xi_i)(1 + \alpha_\eta \eta_i) \tag{21}$$

where

$$\alpha_\xi = \coth(P_\xi/2) - 2/P_\xi \tag{22}$$

$$\alpha_\eta = \coth(P_\eta/2) - 2/P_\eta \tag{23}$$

$$P_\xi = \rho c_p u_\eta h_\xi/\kappa \tag{24}$$

$$P_\eta = \rho c_p u_\eta h_\eta/\kappa \tag{25}$$

$$u_\xi = \mathbf{u}\cdot\mathbf{n}_\xi \tag{26}$$

$$u_\eta = \mathbf{u}\cdot\mathbf{n}_\eta \tag{27}$$

$P_\xi$ and $P_\eta$ are directional Peclet numbers, whilst $\xi_i$ and $\eta_i$ are the isoparametric coordinates for node $i$. The lengths $h_\xi$, $h_\eta$ and the unit vectors $\mathbf{n}_\xi$, $\mathbf{n}_\eta$ are determined by the midside points, as shown in figure 3.

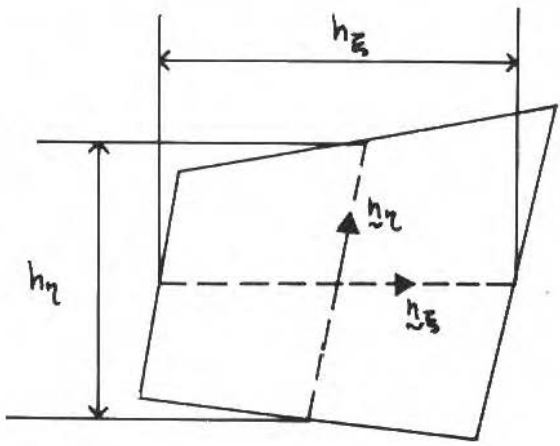


Figure 3. Typical two-dimensional element.

From the definition of the modifying functio we see that the procedure tends to the Galerkin method as the convective terms diminish. On the other hand, our main interest here is to analyse the behaviour of the algorithm when convection is dominant. Figure 4 presents stencils obtained using bilinear Lagrangian elements and $f_i$ defined by equation (21), on a uniform mesh, for pure convection and no source term. For comparison, figure 5 shows the stencils corresponding to the classical 'upwind' finite-difference scheme. Note that the stencils are normalised with respect to the central coefficient. The flow directions considered are $\theta = 0$ and $\theta = 45^0$.

The finite-difference 'upwind' scheme preserves the diagonal dominance property in all cases, preventing the development of unrealistic oscillations. For $\theta = 0$ the scheme gives exact results, corresponding to a node to node propagation of the convected quantity. Nevertheless, for $\theta = 45^0$, excessive diffusion is introduced as there is no contribution from the node at left-bottom corner. In fact, figure 5 shows that such a contribution is replaced by contributions from neighbouring nodes.

On the otherhand, when the Petrov-Galerkin method is used, diagonal dominance and exact propagation occurs for $\theta = 45^0$, but the diagonal

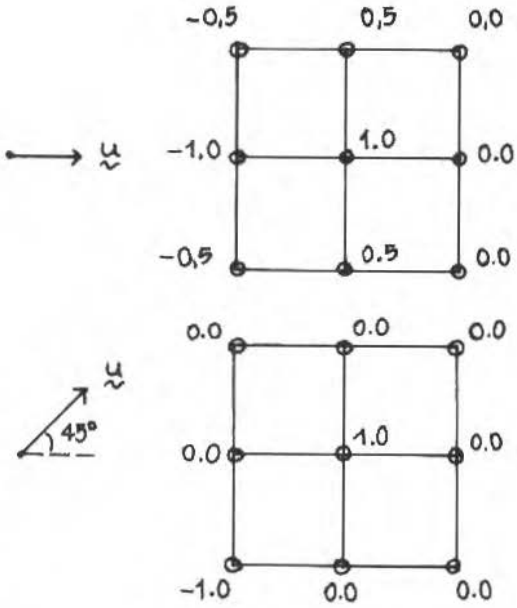


Figure 4. Stencils for pure convection obtained with the present Petrov-Galerkin method.

dominance property is violated for $\theta = 0$. In this case nodal oscillations can arise from unresolved sharp layers.

Having analysed the stencils in figures 4 and 5, it is a simple matter to derive an approximation for the streamline derivative $\partial T/\partial s$, which blends the good propagation properties of the finite-difference 'upwind' for $\theta = 0$ with those of the present method for $\theta = 45^0$.

Consider, for instance, the assembly of elements shown in figure 6.

The convective term is rewritten as

$$\int_{\Omega_e} \phi f \, \rho c_p u_s \, \frac{\partial T}{\partial s} \, d\Omega$$

where $u$, is the modulus of the velocity vector.

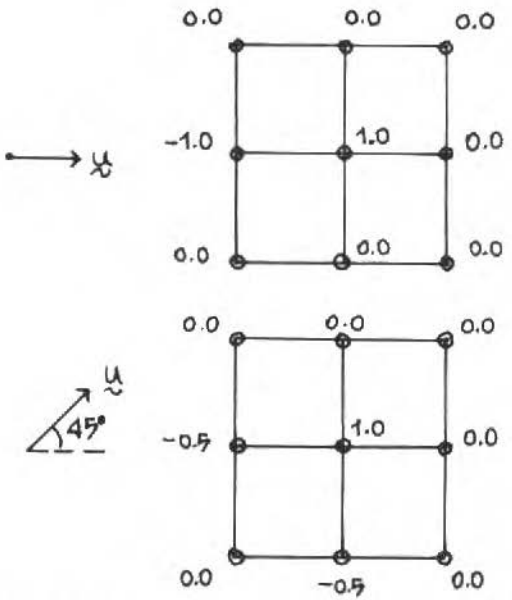


Figure 5. Stencils for pure convection obtained with the 'upwind' finite-difference scheme.

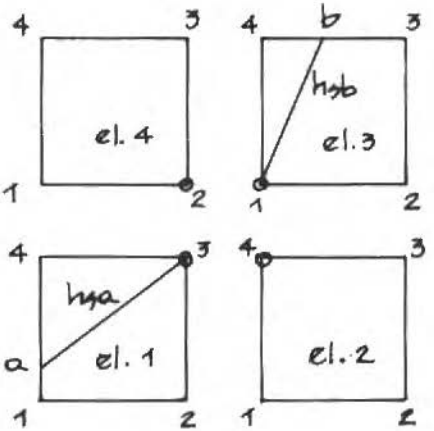


Figure 6. Assembly of elements and approximated streamline.

The streamline derivative for the node being assembled is approximated by

$$\frac{\partial T}{\partial s} = \begin{cases} (T_3 - T_a)/h_{sa} & \text{over element 1.} \\ (T_b - T_1)/h_{sb} & \text{over element 3.} \end{cases}$$

The lengths $h_{sa}$ and $h_{sb}$ approximate the streamline over the assembly and are determined from the flow direction and the element geometry. The temperatures $T_a$ and $T_b$ are interpolated from nodal values, using the bilinear shape functions.

Note that the above treatment of the streamline derivative does not affect nor produces the 'upwinding'. This is in fact introduced by the modifying function, which is consistently applied to the whole equation.

For pure convection exact results are obtained whenever element nodes lie over streamlines ($\theta = 0$ and $\theta = 45^0$ in the case presented earlier, for instance). In general some numerical diffusion will be introduced by the interporlation process. Nevertheless, this is much smaller than the numerical diffusion arising from the classical 'upwind' scheme, which never uses 'corner' nodes to represent $\partial T/\partial s$.

The algorithm obtained using the piecewise continuous modifying function and the above treatment of the streamline derivative preserves diagonal dominance in all cases. This prevents the occurrence of unrealistic solutions and enhances the possibilities of using iterative solvers.

## NUMERICAL EXAMPLES

It was shown in section 2 that the new Petrov-Galerkin formulation produces the so-called 'optimal upwind' scheme and nodally exact solutions for one-dimensional problems. Here our attention goes to two-dimensional cases, where numerical diffusion and oscillation-free results become the main issues.

A variation of the problem presented in [4] has been used to test the performance of the present method in a highly convective situation ($P = 1000$). The domain is the square with side 1.0 and a $20 \times 20$ uniform mesh is employed. Dirichlet boundary conditions are imposed, as shown in figure 7.

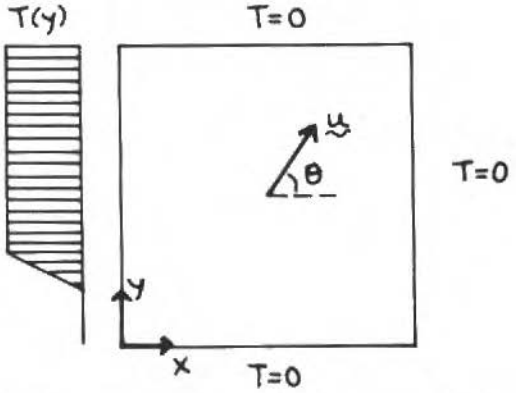


Figure 7. Boundary conditions for test problem.

The profile $T(y)$ shown in figure 7 is zero for $y < 0.2$, one for $y > 0.3$ and varies linearly from zero to one for $0.2 \leq y \leq 0.3$.

It is clear that for large Peclet numbers the steep temperature profile specified at the inlet is propagated downflow. At the same time, the downflow boundary conditions must be satisfied, which causes the formation of boundary-layers.

Although the mesh used is too coarse to capture the detailed features of such boundary-layers, the solutions achieved are virtually exact at nodes for $\theta = 0$ and $\theta = 45^0$. This is expected, as the nodes lie over streamlines for these angles. for other flow directions some numerical diffusion is introduced by the interpolation process. Figure 8 presents the solutions obtained for $\theta = 45^0$ and $\theta = 60^0$. Note that even in the latter case the result is reasonably sharp oscillation-free.

## CONCLUDING REMARKS

A new Petrov-Galerkin formulation has been derived from the concept of locally enforcing self-adjointness.

For one-dimensional problems the 'optimal upwind' scheme has been obtained without using previous knowledge of the analytical solution.

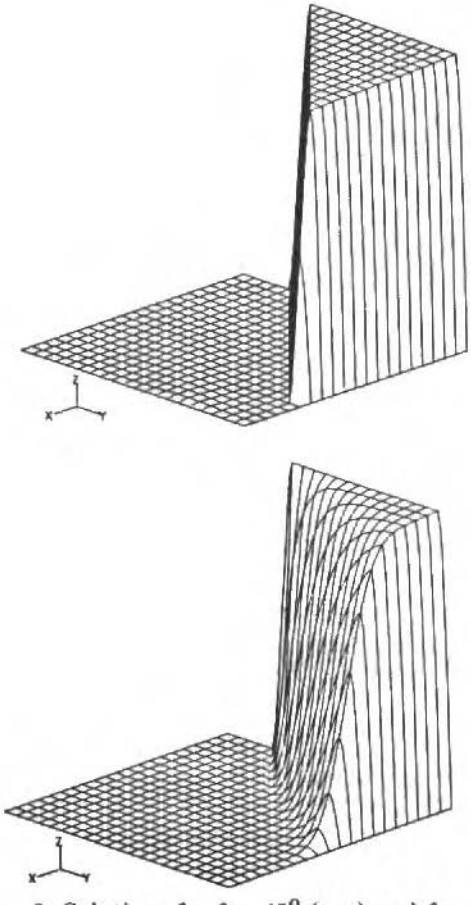

Figure 8. Solutions for $\theta = 45^0$ (top) and $\theta = 60^0$ (bottom).

In two-dimensional cases a special treatment of the streamline deriyative is needed in order to guarantee oscillation-free results and diagonal dominance of the equation system. Accurate results for strong convective problems are obtained, specially when nodes lie over streamlines.

As the diagonal dominance property is preserved, efficient iterative methods (like multigrid techniques) can be used together with the formulation presented.

## ACKNOWLEDGEMENTS

The author would like to thank Prof. O.C. Zienkiewicz and Dr. N.P. Weatherill for the interesting discussions about the subject.

The support of the Brazillian government via CAPES Proc. 402/87-5 is kindly acknowledged.

## REFERENCES

[1] MORTON, K.W. Generalised Galerkin Methods for Esteady and Unsteady Problems'. In: *Numerical Methods for Fluid Dynamics*, (K.W. Morton and M.J. Baines, Eds), Academic Press, 1–32, 1982.

[2] HEINRICH, J.C.; HUYAKORN, P.S.; ZIENKIEWICZ & MITCHELL, A.R. An Upwind Finite Element Scheme for Two-Dimensional Convective Transport Equations, Int. Journal for Num. Meth. in Engng., vol. 11, pp. 131–143, 1977.

[3] HEINRICH, J.C. & ZIENKIEWICZ, O.C. Quadratic Finite Elements Schemes for Two-Dimensional Convective Transport Problems, Int. Journal for Num. Meth. in Engng., vol.11, pp. 1831–1844, 1977.

[4] BROOKS, A.N. & HUGHES, T.J.R. Streamline Upwind/Petrov-Galerkin Formulations for Convection Dominated Flows with Particular Emphasis on the Incompressible Navier-Stokes Equations, Camp. Meth. in Applied Mech. and Engng., vol.32, pp. 199–259, 1982.

[5] KELLY, D.W.; NAKAZAWA, S. & ZIENKIEWICZ, O.C. A Note Upwinding and Anisotropic Balancing Dissipation in Finite Element Approximations to Convective Diffusion Problems, Int. J. Num. Meth. in Engng., vol.15, pp. 1705–1711, 1980.

[6] HUGHES, T.J.R.; MALLET, M. & MIZUKAMI, A. A New Finite Element Formulation for Computational Fluid Dynamics: II. Beyond SUPG, Comp. Meth. in Appl. Mech. and Engng., vol.54, pp. 341–355, 1986.

[7] GALEAO, A.C. & DUTRA DO CARMO, E.G. A Consistent Approximate Upwind Petrov-Galerkin Method for Convection-Dominated Problems, Comp. Meth. in Appl. Mech. and Engng., vol.68, pp. 83–95, 1988.

[8] GUYMON, G.L.; SCOTT, V.H. & HERMANN, L.R. A General Numerical Solution of the Two-Dimensional Diffusion-Convection Equation by the Finite Element Method, Water Res. Res. vol.6., pp. 1611–1615, 1970.

[9] SAMPAIO, P.A.B. A Modified Operator Analysis of Convection Diffusion Problems. Proccedings of the II National Meeting on Thermal Sciences, Águas de Lindóia (Brasil), 180–183, 1988.

[10] SAMPAIO, P.A.B. A Petrov-Galerkin/Modified Operator Formulation for Convection-Diffusion Problems, Int. Journal for Num. Meth. in Engng., vol. 30, pp. 331-347, 1990.

[11] HUGHES, T.J.R. & BROOKS, A. A Theoretical Framework for Petrov-Galerkin Methods with Discontinous Weghting Functions: Application to the Streamline Upwind Procedure. In: Finite Elements in Fluids, vol.4 (R.H. Gallagher et al, Eds), Wiley, pp. 47–65, 1982.

[12] ZIENKIEWICZ, O.C. The Finite Element Method, 3rd ed., McGraw-Hill, 1977.

RBCM – J. of the Braz.Soc.Mech.Sc.
*Vol.XII - nº 3 - pp. 287-299 - 1990*

ISSN 0100-7386
Impresso no Brasil

# EFEITO MAGNUS: SUA UTILIZAÇÃO NA CONVERSÃO DA ENERGIA CINÉTICA DE UMA CORRENTE DE ÁGUA

## *MAGNUS EFFECT: ITS USE ON THE CONVERSION OF ENERGY OF A WATER FLOW*

**Miguel H. Hirata, Atila P. Silva Freire e Jian Su**
Laboratório de Mecânica dos Fluidos/Aerodinâmica
Programa de Engenharia Mecânica, COPPE – UFRJ
C.P. 68506, 21945 Rio de Janeiro RJ

### RESUMO

*Propõe-se um mecanismo para o aproveitamento da energia cinética contida num fluxo de água, que pode ser um rio, um canal, etc. O mecanismo é baseado na força de sustentação que atua em cilindros girantes, os quais possuem alto $C_L$. Uma análise hidrodinâmica preliminar é feita e resultados numéricos são apresentados.*

**Palavras-chave**: Efeito Magnus ▪ Conversão de Energia ▪ Energia Renovável ▪ Dispositivo com Alta Força de Sustentação ▪ Cilindro Girante

### ABSTRACT

*This work presents a theory for the modelling of a mechanical system used on the conversion of water flow kinetic energy. The system explores the hight lift forces resulting from two columns of rotating cylinders in a stream due to the Magnus effect.*

*A difficulty commonly associated with systems that use the Magnus effect is the mechanical arrangement since these systems present combined moves rotation and translation of the cylinders. The present proposal deals with a mechanical system where the cylinders are supported at both ends, and hence, contrary to other configurations, do not work in balance.*

*The hydrodynamic analysis presented here is based on the actuator disk theory, for the farfield, combined with a description of the flow field around a cylinder element.*

**Keywords**: Magnus Effect ▪ Energy Conversion ▪ Renewable Energy ▪ High Lift Device ▪ Rotating Cylinder

Submetido em Abril/90 Aceito em Agosto/90

## INTRODUÇÃO

Neste trabalho apresentamos uma proposta para o aproveitamente da energia cinética contida num fluxo de água, que pode ser um rio, um canal, etc. Para a extração desta energia é proposto um mecanismo baseado na força de sustentação, resultante do movimento de rotação de um cilindro imerso numa corrente fluida (Efeito Magnus). A principal vantagem deste tipo de mecanismo reside no fato de que o coeficiente de sustentação ($C_L$) para cilindros girantes poder atingir valores maiores que dez, ao passo que os melhores perfis aerodinâmicos dificilmente podem trabalhar com valores superiores a dois; é claro que estes cilindros apresentam, também, elevados valores do coeficiente de arrasto ($C_D$) mas, mesmo assim, os resultados podem ser animadores. Cabe ressaltar que mesmo considerando a força de sustentação, e não o seu coeficiente, ainda se pode esperar resultados compensadores (note que o coef. de sustentação é definido com base no diâmetro, no caso do cilindro, e, no caso do perfil, com base no seu comprimento).

Uma dificuldade inerente aos mecanismos que utilizam o Efeito Magnus está associada aos aspectos mecânicos, uma vez que os cilindros devem apresentar um movimento de rotação combinado com um de translação. O mecanismo proposto - veja Fig. 1 - apresenta como atrativo principal múltiplos cilindros girantes, que são apoiados em mancais nas duas extremidades; não trabalham, portanto, em balanço.

Além da configuração proposta apresentamos uma análise básica que, como uma primeira aproximação, deve simular razoavelmente os fenômenos hidrodinâmicos. Esta análise utiliza a teoria do disco atuador (Rankine) combinada com uma versão da teoria do elemento de pá, e não leva em consideração a influência das paredes, a interação entre os cilindros adjacentes e o desempenho de cilindros operando na esteira de outros cilindros (aliás este é um assunto de investigação básica em hidrodinâmica).

Não houve a preocupação com a análise mecânica do dispositivo, com os aspectos relacionados com o projeto e com a otimização. Os esforços tiveram como objetivo principal a análise hidrodinâmica, que possui como intuito motivar a procura de mecanismos que façam uso do alto coeficiente de sustentação dos cilindros girantes.

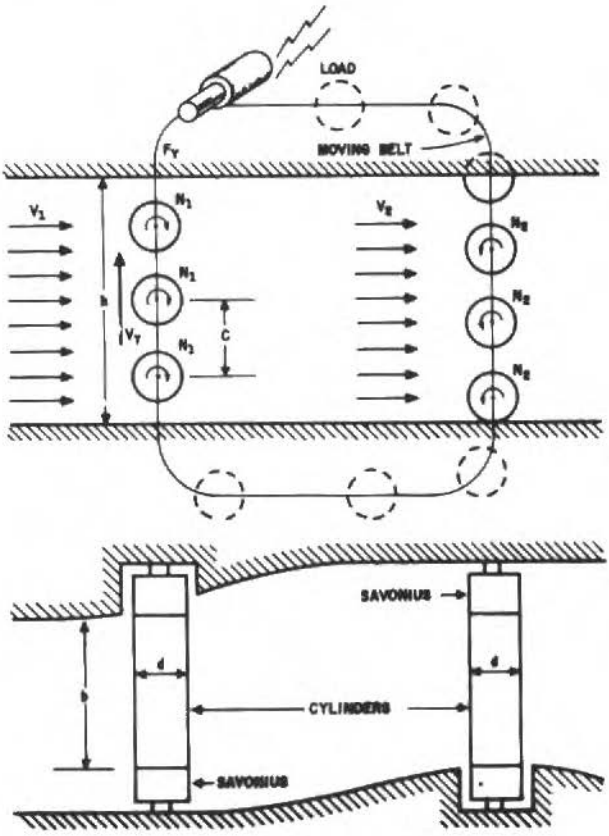


Figura 1. The proposed system.

## O MECANISMO PROPOSTO

Vários mecanismos foram propostos para a utilização do efeito Magnus no aproveitamento da energia dos ventos. Um deles [1] propõe a utilização de cilindros girantes, com o eixo vertical, sobre uma plataforma que se desloca em círculos sobre trilhos, enquanto que outro [2] propõe a substituição das pás de um rotor eólico de eixo horizontal por cilindros girantes; certamente outros mecanismos propostos existem.

A Fig. 1 mostra esquematicamente o mecanismo proposto. Este consta de um canal e transversalmente a ele duas séries de cilindros girantes que são interconectados, nas suas extremidades, por correias que também acionam a carga (gerador, bomba, etc). Observemos que os cilindros da segunda coluna (cilindros de juzante) devem girar em sentido oposto ao dos cilindros da primeira coluna. Existem diferentes maneiras para imprimir o movimento de rotação nos cilindros; pode-se propor, como na figura, que este movimento seja propiciado por rotores do tipo Savonius localizados nas extremidades dos cilindros.

## ANÁLISE HIDRODINÂMICA

A análise hidrodinâmica do mecanismo proposto é dividida em três partes. A primeira, equivalente ao campo externo, trata dos aspectos globais; a segunda, analisa o escoamento junto aos cilindros, o que corresponde a teoria do elemento de pá da análise de rotores eólicos de eixo horizontal; a terceira combina os resultados das duas primeiras.

### Modelo do Disco Atuador

(TVQM - Teoria da Variação da Quantidade de Movimento)

A análise dos aspectos globais é feita com a utilização do princípio da conservação da quantidade de movimento, que constitui-se na base da teoria (modelo) do disco atuador ou de Rankine.

O modelo do disco atuador é esquematizado na Fig. 2 e tem como resultado de maior interesse para a presente análise a relação:

$$V = \frac{V_0 + V_4}{2}\,, \tag{1}$$

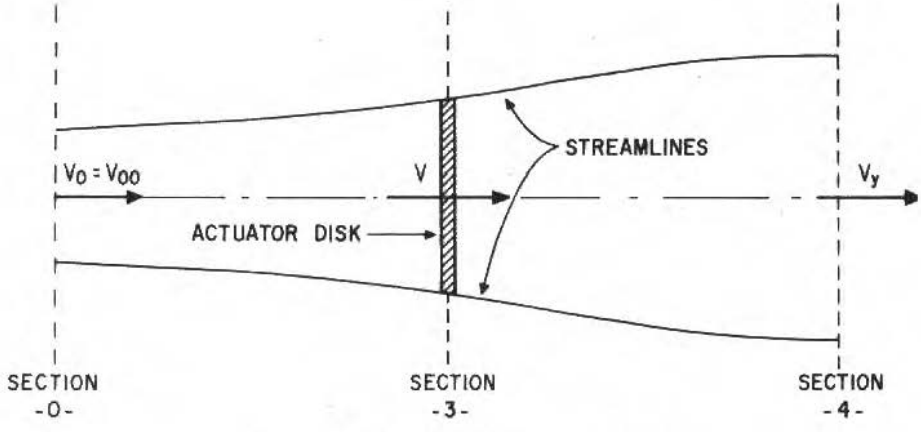


Figura 2. Theory of the actuator disk.

Esta relação mostra que metade da variação da velocidade ocorre antes do disco. Como é bem conhecido, este modelo utiliza hipóteses bastante generosas, mas que, no entanto, parecem suficientes para a presente análise.

Uma análise elementar do balanço de energia mostra que $V_4 < V_0$ e o princípio da conservação da massa exige que a área da seção – 4 – seja maior que aquela da seção – 0 –, considerada a montante do disco. O fator de indução da velocidade axial – $a$ – pode ser definido como:

$$V_4 = V_0(1 - a) \,. \tag{2}$$

## Análise do Escoamento Junto aos Cilindros

(TEP-Teoria do Elemento de Pá)

A análise do escoamento junto aos cilindros e os resultados acima mencionados devem fornecer as equações necessárias para os nossos propósitos. Esta deve iniciar-se com o estudo do diagrama de velocidades e forças que atuam sobre um cilindro, como mostra a Fig. 3. Esta figura refere-se a um cilindro da coluna (1) - coluna de cilindros a montante - que se move na direção de $y$ positivo com velocidade de transição $V_T$. Como a velocidade incidente é indicada por $V_1$ a velocidade resultante $V_{R1}$, que forma um ângulo $\alpha_1$ com o eixo dos $x$, é definida como:

$$V_{R1} = \sqrt{V_1^2 + V_T^2} \,. \tag{3}$$

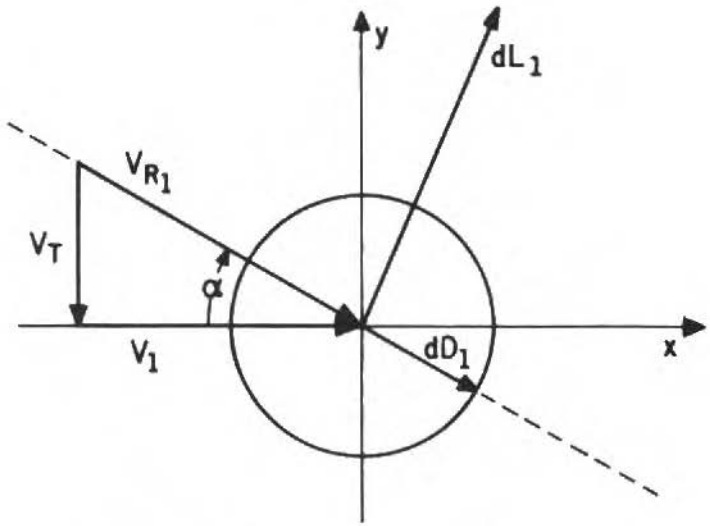


Figura 3. Diagram of forces and velocities.

A força hidrodinâmica resultante é decomposta nas componentes ortogonais $dL_1$ e $dD_1$, conforme indicado na Fig. 3. A projeção destas forças sobre o eixo $x$ será relevante para a análise do item seguinte e aquela sobre $y$ será responsável pela produção de trabalho útil.

Temos, então:

$$d\phi_{1x} = dL_1 \sin\alpha_1 + dD_1 \cos\alpha_1 \ , \tag{4}$$

$$d\phi_{1y} = dL_1 \cos\alpha_1 + dD_1 \cos\alpha_1 \ , \tag{5}$$

onde

$$2dL = C_{L1}\rho V_{R1}^2 d \cdot dz \quad ; \quad C_{L1} = f(V_{R1}, N_1)$$

$$2dD = C_{D1}\rho V_{R1}^2 d \cdot dz \quad ; \quad C_{D1} = g(V_{R1}, N_1)$$

e

$N$ = rotação imprimida aos cilindros

Observemos que uma análise análoga pode ser efetuada para um cilindro da coluna 2 (coluna de cilindros a jusante). A única diferença, além dos valores das variáveis, encontra-se na direção de $V_T$, que é oposta aquela dos cilindros da coluna 1, vide Fig. 1.

A força total que atua em cada coluna de $Z_i (i = 1, 2)$ cilindros é dada por:

$$F_{ix} = Z_i \int_0^b d\phi_{1x} = \frac{Z_i}{V_{Ri}} \left[L_i V_T + D_i V_i\right] \ , \tag{6}$$

$$F_{iy} = Z_i \int_0^b d\phi_{1y} = \frac{Z_i}{V_{Ri}} \left[L_i V_i - D_i V_T\right] \ , \tag{7}$$

onde $b$ = comprimento dos cilindros. Para a completa determinação de $F_{ix}$ e $F_{iy}$ torna-se necessário uma informação adicional, além daquelas sobre o comportamento de $C_L$ e $C_D$, assim:

- Velocidade incidente $V_i$, $i = 1, 2$ - assumimos que a velocidade incidente nos cilindros, de ambas as colunas, seja fornecida pela velocidade $V$, fornecida pela expressão (1), isto é, a velocidade no disco - veja figura 2.

$$V = V_1 = V_2 \ . \tag{8}$$

- O coeficiente de sustentação e o de arrasto assumem a forma [3], [4]

$$C_L = 1 + 3(\sigma - 1) \ , \tag{9}$$

$$C_D = 0.239\ \sigma^2 \ , \tag{10}$$

onde o coeficiente de rotação - $\sigma$ - é definido como

$$\sigma = \frac{\omega R}{V_r} \ . \tag{11}$$

## TVQM Combinada com TEP

O princípio de variação da quantidade de movimento, utilizado na obtenção da expressão (1) fornece, também:

$$F_{1x} + F_{2x} = \dot{m}(V_0 - V_4) \ ,$$

onde $\dot{m}$ = vazão mássica. Com auxílio de (1) obtemos:

$$F_{1x} + F_{2x} = \frac{\rho b h}{2} \ [V_0 + V_4][V_0 - V_4] \ , \tag{12}$$

A expressão (8) nos sugere uma série de outros resultados:

a) $V_R = V_{R1} = V_{R2}$ uma vez que $V_T = V_{T1} = V_{T2}$,

b) $L = L_1 = L_2$ e $D = D_1 = D_2$ uma vez que os cilindros possuem o mesmo diâmetro e comprimento, além da rotação $N = N_1 = N_2$,

c) $F_x = F_{1x} = F_{2x}$ e $F_y = F_{1y} = F_{2y}$,

d) $Z = Z_1 = Z_2$.

Levando estas relações em (12) e utilizando (6) temos:

$$8\lambda \ \frac{V_R}{C_0}\left[C_L \ \frac{V_T}{V_0} + C_D \ \frac{V}{V_0}\right] = \left[1 + \frac{V_4}{V_0}\right]\left[1 - \frac{V_4}{V_0}\right] \ , \tag{13}$$

onde a razão de áreas - $\lambda$ - é definida como

$$\lambda = Z \ d/h \ . \tag{14}$$

A seguir as velocidades são adimensionalizadas com base em $V_0$ e indicadas por um ('), isto é:

$$V' = V/V_0 \quad , \quad V'_T = V_T/V_0 \ , \quad \text{etc,}$$

o que facilita os trabalhos numéricos e os desenvolvimentos futuros. A expressão (13), juntamente com (1) e (3) nos permitem a obtenção de $V$ e $V_R$ se forem conhecidos $\lambda$, $\sigma$ e $V_T$, e, por esta razão, são transcritas abaixo

$$2V' = V_0' + V_4' \,, \tag{1'}$$

$$V_R' = \sqrt{V'^2 + V_T'^2} \,, \tag{3'}$$

$$2\lambda V_R'[C_L V_T' + C_D V'] = [1 - V_4'][1 + V_4'] \,. \tag{13'}$$

## FORÇA E POTÊNCIA

Para o dimensionamento do sistema e para a análise de seu desempenho é necessário a estima da força total na direção $y$ e da potência disponível. Se $b$ for mantido constante o valor de $h$ na seção - 2 -, onde se deslocam os cilindros de jusante, deve ser diferente daquele na seção - 1 -, onde se deslocam os cilindros de montante. Aqui assumiremos que esta diferença seja pequena e tomamos o valor da seção - 1 -. Assim, o coeficiente de força - $C_F$ - é definido como

$$C_F = \frac{F_{1y} + F_{2y}}{\frac{1}{2}\,\rho V_0^2 bh} \,. \tag{15}$$

A substituição de (6) e (7) na definição acima fornece

$$C_F = 2\lambda V_R'[C_L V' - C_D V_T'] \,, \tag{16}$$

que é a expressão utilizada para o cálculo numérico de $C_F$.

O coeficiente de potência - $C_P$ - é definido como:

$$C_P = \frac{P_y}{\frac{1}{2}\,\rho V_0^3 bh} \,, \tag{17}$$

e seu cálculo pode ser efetuado lembrando que

$$P_u = 2F_y V_T = \text{potência útil.}$$

Tem-se, portanto

$$C_P = 2\lambda V_T' v_R'[C_L V' + C_D V_T'] \,, \tag{18}$$

que é a expressão utilizada para o cálculo numérico de $C_P$. Observemos que esta grandeza representa o rendimento do sistema.

## RESULTADOS NUMÉRICOS E EXEMPLO DE APLICAÇÃO

As expressões (16) e (18) são utilizadas no cálculo numérico dos coeficientes de força e potência. Note-se que para a utilização destas expressões o sistema de equações $(1'), (3')$ e $(13')$ deve ser resolvido.

As figuras 4 a 9 mostram resultados para diferentes combinações dos parâmetros $\lambda$ e $\sigma$. Estas figuras são de utilidade no dimensionamento do sistema.

Como exemplo de aplicação, consideremos um canal de seção retangular $(b \times h)$, por onde escoa água com velocidade $V_0$.

A estima da potência do mecanismo a ser instalado pode ser feita com a utilização de (17) assumindo-se um valor típico de $C_P = 0,4$, como mostram os gráficos.

A melhor razão de transmissão pode ser obtida a partir do coeficiente de força exigido pela carga (definido de maneira análoga a expressão (14)), com a utilização dos gráficos.

Observe que o coeficiente de rotação utilizado - $\sigma$ - permitirá definir a grandeza $N$.

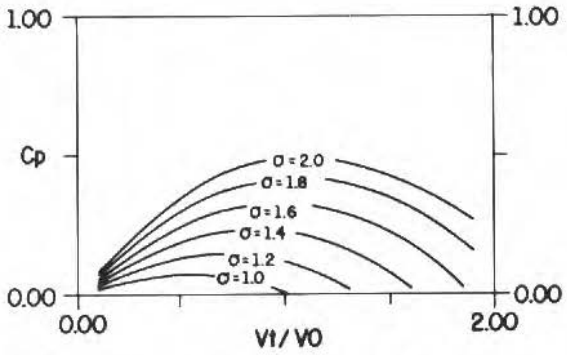


Figura 4. Force coefficient for $Zd/h = 0.10$.

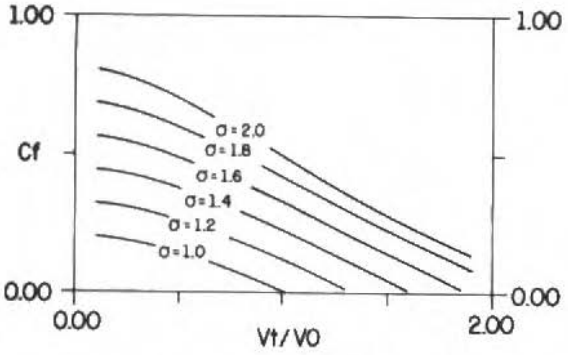


Figura 5. Power coefficient for $Zd/h = 0.10$.

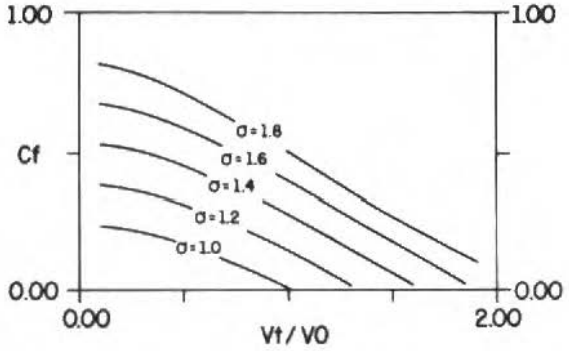


Figura 6. Force coefficient for $Zd/h = 0.12$.

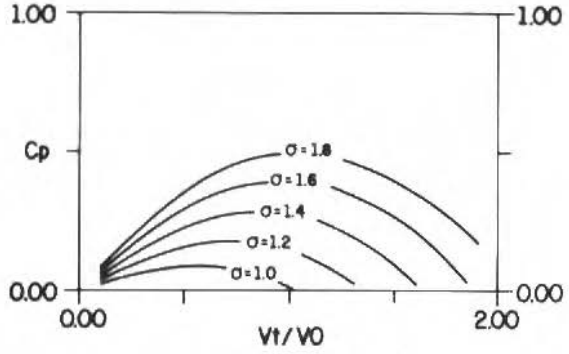


Figura 7. Power coefficient for $Zd/h = 0.12$.

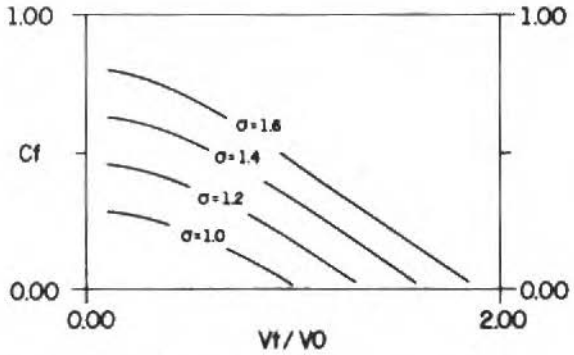


Figura 8. Force coefficient for $Zd/h = 0.14$.

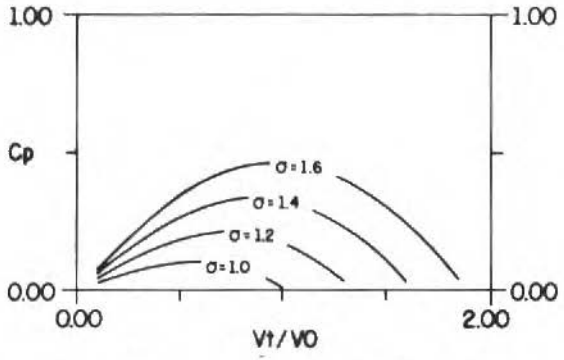


Figura 9. Power coefficient for $Zd/h = 0.14$.

## CONCLUSÕES

A análise hidrodinâmica mostra as potencialidades do mecanismo proposto; no entanto, é oportuno ressaltar algumas características inerentes a esta proposta.

- embora as velocidades das correntes disponíveis de água sejam baixas, quando comparadas com as velocidades dos ventos, a massa específica da água é alta (aproximadamente 1000 vezes a do ar) o que deve contrabalançar

na estima da potência.

- normalmente a velocidade das correntes de água é relativamente constante, quando comparada com a velocidade do vento.

- o mecanismo, em princípio, não exige a construção de barragens.

É importante ressaltar, também, que a análise apresentada possui limitações impostas pela simplicidade do modelo utilizado. As hipóteses utilizadas foram mencionadas no texto e mostram que a análise deve ser considerada como preliminar. No momento, esforços estão sendo dispendidos no sentido de relaxar algumas hipóteses e assim propor um modelo mais complexo.

## REFERÊNCIAS

[1] CORREA, C.J. Estudo Experimental do Efeito Magnus, Tese de Mestrado, Dept. Eng. Mec. - PUC/RJ, 1985.

[2] ELDRIGE, F.R. Wind Machines, National Science Foundation, USA, 1975.

[3] HIRATA, M.H. & MANSOUR, W.M. Potentials and Limitations of Wind Energy, Academia Brasileira de Ciências, 1978.

[4] SWANSON, W.M. The Magnus Effect: a Summary of Investigations to Date, J. of Basic Engineering, September, 1961.

**RBCM – J. of the Braz.Soc.Mech.Sc.** ISSN 0100-7386
*Vol.XII - nº 3 - pp. 301-310 - 1990* Impresso no Brasil

# UNIFIED INTEGRAL TRANSFORM METHOD

## *MÉTODO DA TRANSFORMADA INTEGRAL UNIFICADO*

**M.D. Mikhailov***
**R.M. Cotta****
EE/COPPE/UFRJ
Universidade Federal do Rio de Janeiro
Rio de Janeiro RJ, Brazil

*Permanent address:
Institute for Applied Mathematics and Informatics
P.O. Box 384, Sofia 1000, Bulgaria

** Address reprint requests to
Dr. R.M. Cotta
Programa de Engenharia Mecânica
COPPE – Universidade Federal do Rio de Janeiro
Cidade Universitária, C.P. 68503
21945 Rio de Janeiro RJ, Brasil

### ABSTRACT

*The theoretical foundations of the unified integral transform method are presented. The method transforms a non-linear partial differential equation problem to a coupled non-linear system of ordinary differential equations that is to be solved numerically. Also, partial differential eigenvalue problem is transformed to the algebraic one, that can be solved by existing codes.*

**Keywords**: Integral Transform ▪ Numerical Method ▪ Matrix Problem

### RESUMO

*As bases teóricas do método da transformada integral unificado são apresentadas. O método transforma um problema de equação diferencial parcial não-linear em um sistema não-linear acoplado de quações diferenciais ordinárias, que deve ser resolvido numericamente. Além disso, o problema diferencial parcial de autovalor é transformado em um problema algébrico, que pode ser resolvido por códigos já existentes.*

**Palavras-chave**: Transformada Integral ▪ Método Numérico ▪ Problema Matricial

---

Invited Paper by Alvaro T. Prata

## INTRODUCTION

Many engineering problems lead to partial differential equations subjected to initial and boundary conditions. Usually such problems are solved by one of the following numerical methods: finite differences, finite elements, boundary elements, or spectral methods [1,2].

All methods transform the original partial differential equation problem to a set of algebraic or ordinary differential equations.

The finite differences and finite elements methods consider from very begining the field variables in limited number of points in the solution region, while the boundary elements method uses limited number of boundary points. The spectral and integral transform methods use solutions in terms of truncated series, which is somehow analogous to considering limited number of points.

The classical finite integral transform method [3,4] permited to solve only linear problems. Recently various non-linear heat transfer problems were successfuly treated by using a generalized integral transform method. The reader can find these new results in [5].

The goal of this paper is to present theoretical foundations of the unified finite integral transform method.

First, the linear matrix problem is considered for boundary conditions more general than those in [3]. The problem is transformed to the corresponding system of ordinary differential equations in a more ellegant manner than in [4].

Second, the non-linear matrix problem is transformed to a coupled nonlinear system of ordinary differential equations that is to be solved numerically. Then, the desired solution is readily given by the corresponding inversion formula.

Finally, the integral transform technique is used to reduce a given eigenvalue problem described by partial differential equations, to an algebraic one, that can be solved by existing codes.

The unified finite integral transform method presented here is applicable to a large class of field problems including heat conduction, elasticity, acoustics, etc. Current work is done to create automatic software for heat transfer problems.

## LINEAR PROBLEMS

To define and solve a wide class of boundary value problems in a compact and ellegant manner the following matrices are introduced in [6]

$$[D] = [\partial_{ij}] \tag{1.a}$$

and

$$[D_S] = [\ell_{ij}] \tag{1.b}$$

where the elements $\partial_{ij}$ are zero or first-order differential operators defined over the finite domain $V$ bounded by the surface $S$, and $\ell_{ij}$ are the direction cosines of the outward drawn normal to the boundary surface $S$. For example, $\partial_{ij}$ can be zero, $\partial/\partial x$, $\partial/\partial y$, etc.

The above two matrices are used to define the following linear operators

$$\mathcal{L} = -[D]^t[C][D] + [B] \qquad \text{in } V \tag{2.a}$$

$$\mathcal{L}^* = -[D]^t[C]^t[D] + [B]^t \qquad \text{in } V \tag{2.b}$$

$$\beta = -[D_S]^t[C][D] + [A] \qquad \text{in } S \tag{2.c}$$

$$\beta^* = -[D_S]^t[C]^t[D] + [A]^t \qquad \text{in } S \tag{2.d}$$

where the elements of $[C]$ and $[B]$ are known functions in the finite domain $V$, the elements of $[A]$ are known functions on the boundary surface $S$, and the superscript $t$ denotes the transpose of a matrix. Here $\mathcal{L}^*$ and $\beta^*$ are the adjoint operators of the operators $\mathcal{L}$ and $\beta$, respectively. The operators (2.c) and (2.d) are more general than those considered in [4].

The volume and the surface inner products of two column vectors $\{u\}$ and $\{v\}$ are defined as

$$[\{u\},\ \{v\}]_V = \int_V \{u\}^t\ \{v\}\ dV \tag{3.a}$$

$$[\{u\},\ \{v\}]_S = \int_S \{u\}^t\ \{v\}\ dS \tag{3.b}$$

The "transposed" form for two column vectors $\{u\}$ and $\{v\}$, whose elements $u_i$ and $v_i$ $(i = 1, \ldots, n)$ are continuous functions of the space variables in domain $V$ bounded by the surface $S$, is derived by using the same manipulations as in [4]. The result is

$$\left[\{v\},\ \mathcal{L}\{u\}\right]_V + \left[\{v\},\ \beta\{u\}\right]_S = \left[\{u\},\ \mathcal{L}^*\{v\}\right]_V + \left[\{u\},\ \beta^*\{v\}\right]_S \quad (4)$$

Let us consider the following linear boundary value problem

$$\left[[W]\,\mathcal{T} + \mathcal{L}\right]\{\phi\} = \{P\} \qquad \text{in } V \quad (5.a)$$

subject to the boundary and initial conditons

$$\beta\{\phi\} = \{\varphi\} \quad , \qquad \text{on } S \quad (5.b)$$

$$\frac{\partial^p\{\phi\}}{\partial t^p} = \{f\}_p \qquad p = 0, 1, \ldots, (k-1) \text{ at } t = 0 \quad (5.c)$$

where $\mathcal{T}$ denotes a linear differential time operator of order $k$. The elements of $[W]$ and $\{f\}_p$ are known functions over the domain $V$. The source terms $\{P\}$ and $\{\varphi\}$ are known functions of time in $V$ and $S$ respectively. This problem covers as special case a wide number of problems, such as in heat conduction, elasticity, etc.

To solve the problem (5) we need the solution of the following adjoint eigenvalue problems [4]

$$\mathcal{L}\{\psi\} = \lambda[W]\,\{\psi\} \qquad \text{in } V \quad (6.a)$$

$$\beta\{\psi\} = 0 \qquad \text{on } S \quad (6.b)$$

and

$$\mathcal{L}^*\{\psi\}^* = \lambda[W]^t\{\psi\}^* \qquad \text{in } V \quad (7.a)$$

$$\beta^*\{\psi\}^* = 0 \qquad \text{on } S \quad (7.b)$$

The eigenfunctions $\{\psi\}$ and $\{\psi\}^*$ form biorthogonal sets, and any eigenvalue $\lambda_i$ $(i = 1, 2, \ldots, \infty)$ of the system (6) is at the same time an eigenvalue of the adjoint system (7).

The orthogonality condition

$$\left[\{\psi\}_j^*,\ [W]\{\psi\}_i\right]_V = 0 \qquad \text{for } i \neq j \tag{8.a}$$

is developed by using the "transposed" form (4) for $\{u\} = \{\psi\}_i$ and $\{v\} = \{\psi\}_j^*$, and the eigenvalue problems (6) and (7) to evaluate the expression $\mathcal{L}\{\psi\}_i$, $\beta\{\psi\}_i$, $\mathcal{L}^*\{\psi\}_j^*$, $\beta^*\{\psi\}_j^*$, respectively, where the eignefunctions are normalized, i.e.

$$\left[\{\psi\}_i^*,\ [W]\{\psi\}_i\right]_V = 1 \tag{8.b}$$

We assume that the eigenvalues $\lambda_i$ and the corresponding normalized eigenfunctions $\{\psi\}_i$ and $\{\psi\}_j^*$ are known. Then, the solutions of problem (5) can be written in the form

$$\{\phi\} = \sum_{i=1}^{\infty} \{\psi\}_i \tilde{\phi}_i \qquad \text{in } V \tag{9}$$

To determine the expansion coefficients $\tilde{\phi}_i$, both sides of eq.(9) are premultiplied by $\{\psi\}_j^{*t}[W]$, integrated over the region $V$ and the orthogonality relation (8) is utilized. The result is

$$\tilde{\phi}_i = \left[\{\psi\}_i^*,\ [W]\{\phi\}\right]_V \tag{10}$$

This equation defines the finite integral transform $\tilde{\phi}_i$, having the inversion formula (9).

The original problem (5) is transformed into a system of ordinary differential equations by using the "transposed" form (4) for $\{u\} = \{\phi\}$ and $\{v\} = \{\psi\}_i^*$, and eqs. (5.a,b) and (7.a,b) to evaluate the expressions for $\mathcal{L}\{\phi\}$, $\beta\{\phi\}$, $\mathcal{L}^*\{\psi\}_i^*$, $\beta^*\{\psi\}_i^*$, respectively. We obtain the following infinite decoupled system

$$T\tilde{\phi}_i + \lambda_i \tilde{\phi}_i = \left[\{\psi\}_i^*,\ \{\varphi\}\right]_S + \left[\{\psi\}_i^*,\ \{P\}\right]_V \tag{11.a}$$

where $i = 1, 2, \ldots, \infty$.

The initial conditons needed for the solution of eq. (11.a) are obtained by taking the integral transform of the initial conditions (5.c) according to eq. (10). We obtain

$$\frac{d^p\,\bar{\phi}_i}{dt^p} = \left[\{\psi\}_i^*,\ [W]\{f_p\}\right] \qquad \text{at } t = 0 \tag{11.b}$$

The steady state problem

$$\mathcal{L}\{\phi\} = \{P\} \qquad \text{in } V \tag{12.a}$$
$$\beta\{\phi\} = \{\varphi\} \qquad \text{on } S \tag{12.b}$$

can be transformed in the same way to the algebraic equations

$$\lambda_i\,\bar{\phi}_i = \left[\{\psi\}_i^*,\ \{\varphi\}\right]_S + \left[\{\psi\}_i^*,\ \{P\}\right]_V \tag{13}$$

The systems (11) and (13) are to be solved for the finite integral transform $\bar{\phi}_i$. Then the desired solution is readily given by the inversion formula (9). By increasing the number of terms the solution can be obtained with desired accuracy.

The above results give as a very spacial case, the solution of class one problems as described in detail in [5].

## NON-LINEAR PROBLEMS

Let us consider the following problem

$$\left[[W] + [W]_n\right]\,T\{\phi\} + (\mathcal{L} + \mathcal{L}_n)\{\phi\} = \{P\} + \{P\}_n \quad \text{in } V \tag{14.a}$$
$$\left[\beta + \beta_n\right]\,\{\phi\} = \{\varphi\} + \{\varphi\}_n \qquad \text{on } S \tag{14.b}$$

$$\frac{\partial^p\{\phi\}}{\partial t^p} = \{f\}_p \quad p = 0, 1, \ldots, (k-1) \qquad \text{at } t = 0 \tag{14.c}$$

The problem (14) is an extension of problem (5). Several non-linear terms having index '$n$' are added. $\mathcal{L}_n$ and $\beta_n$ are operators similar to those given

by eq.(2) but with coefficients that vary not only in space but also depend on time and on the field variable $\{\phi\}$. The source terms $\{P\}_n$ and $\{\varphi\}_n$ are also nonlinear since they depend on space, time, and the field variable $\{\phi\}$.

We assume that linear terms represent problem (14) in some average sense and consider all nonlinear terms as source terms. Then, problem (14) is rewriten as

$$[W]\,\mathcal{T}\{\phi\} + \mathcal{L}\{\phi\} = \{P\}_{eff} \qquad \text{in } V \qquad (15.a)$$

$$\beta\{\phi\} = \{\varphi\}_{eff} \qquad \text{on } S \qquad (15.b)$$

$$\frac{\partial^p\{\phi\}}{\partial t^p} = \{f\}_p \quad p = 0, 1, \ldots, (k-1) \qquad \text{at } t = 0 \qquad (15.c)$$

where

$$\{P\}_{eff} = \{P\} + \{P\}_n - [W]_n\,\mathcal{T}\{\phi\} - \mathcal{L}_n\{\phi\} \qquad (16.a)$$

$$\{\varphi\}_{eff} = \{\varphi\} + \{\varphi\}_n - \beta_n\{\phi\} \qquad (16.b)$$

The problem (15) can be transformed to the $\tilde{\phi}_i$ variables by using directly eqs.(11). The field variable $\{\phi\}$ is to be removed from the source terms $\{P\}_{eff}$ and $\{\varphi\}_{eff}$ by using the truncated to the $n$-th term inversion formula (9). In this way a coupled nonlinear system of ordinary differential equations is obtained that has to be solved numerically. Subroutines that can be used are described in [5]. Once the finite integral transform $\tilde{\phi}_i$ is numerically obtained, then the desired solution is readily given by the inversion formula (9).

The convergence of the inversion formula (9) is improved when the boundary conditon (5.b) is made homogeneous. In many cases it is possible to obtain homogeneous boundary conditions by splitting the solution into two parts

$$\{\phi\} = \{u\} + \{v\} \qquad (17)$$

The first one is to satisfy the nonhomogeneous boundary conditions

$$\beta\{u\} = \{\varphi\} + \{\varphi\}_n - \beta_n\{\phi\} \qquad (18)$$

The second one is defined by

$$[W]\,\mathcal{T}\{v\} + \mathcal{L}\{v\} = \{P\}_{eff} \qquad \text{in } V \qquad (19.a)$$

$$\beta\{v\} = 0 \qquad \text{on } S \qquad (19.b)$$

$$\frac{\partial^p\{v\}}{\partial t^p} = \{f\}_p - \frac{\partial^p\{u\}}{\partial t^p}\ , \quad p = 0, 1, \ldots, (k-1) \quad \text{at } t = 0 \qquad (19.c)$$

where

$$\{P\}_{eff} = \{P\} + \{P\}_n - [W]\,\mathcal{T}\{u\} - [W]_n\,\mathcal{T}(\{u\} + \{v\}) - \mathcal{L}\{u\} - \\ -_{\setminus}(\{\sqcap\} + \{\sqsubseteq\}) \qquad (19.d)$$

We have some freedom in selecting $\{u\}$. The computations are facilitated if $\{u\}$ is sellected in such a way that some of the terms in $\{P\}_{eff}$ become zero.

Problem (19) can be transformed to a coupled system of ordinary differential equations by using directly eqs.(11). But now the convergence is improved since the surface integral is missing.

Once the finite integral transform $\bar{v}_i$ is numerically obtained, then the desired solution is given by the inversion formula

$$\{v\} = \sum_{i=1}^{n} \{\psi\}_i\ \bar{v}_i \qquad (20)$$

By increasing the number of terms we can obtain the results with prescribed accuracy.

## EIGENVALUE PROBLEM

Let us consider the following problem

$$\mathcal{L}_1\{\Omega\} = \nu[W]_1\{\Omega\} \qquad \text{in } V \qquad (21.a)$$

$$\beta_1\{\Omega\} = 0 \qquad \text{on } S \qquad (21.b)$$

where the operators $\mathcal{L}_1$ and $\beta_1$ are similar to those described by eqs.(2.a) and (2.c) but the matrices $[A]$, $[B]$, $[C]$ are replaced by the known matrices $[A]_1$,

$[B]_1$ and $[C]_1$. The eigenvalues $\nu$ and the eigenfunctions $\{\Omega\}$ are unknown. Our goal is to develop a method for their computation.

We rearrange eqs. (21) to be analogous to the steady state problem (12). Problem (21) is rewritten as

$$\mathcal{L}\{\Omega\} = (\mathcal{L} - \mathcal{L}_1)\{\Omega\} + \nu[W]_1\{\Omega\} \qquad \text{in } V \qquad (22.a)$$

$$\beta\{\Omega\} = (\beta - \beta_1)\{\Omega\} \qquad \text{on } S \qquad (22.b)$$

The comparison of problems (12) and (21) gives

$$\{\phi\} = \{\Omega\},\ \{P\} = \left[(\mathcal{L} - \mathcal{L}_1) + \nu[W]_1\right]\{\Omega\},\ \{\varphi\} = (\beta - \beta_1)\{\Omega\} \qquad (23)$$

By using these results into eqs. (13) we obtain the algebraic system

$$\lambda_i\widetilde{\Omega}_i = \left[\{\psi\}_i^*,\ (\beta - \beta_1)\{\Omega\}\right]_S + \left[\{\psi\}_i^*,\ (\mathcal{L} - \mathcal{L}_1)\{\Omega\}\right]_V + \\ + \nu\left[\{\psi\}_i^*,\ [W]_1\{\Omega\}\right]_V \qquad (24)$$

We introduce into eq. (24) the truncated to the $n$-th term inversion formula

$$\{\Omega\} = \sum_{j=1}^{n}\{\psi\}_j\,\widetilde{\Omega}_j \qquad (25)$$

The resulting system is written in matrix form as

$$\left[[A] + [\lambda]\right]\{\widetilde{\Omega}\} = \nu[B]\{\widetilde{\Omega}\} \qquad (26)$$

where $\{\widetilde{\Omega}\}^t = [\widetilde{\Omega}_1,\ \widetilde{\Omega}_2, \ldots, \widetilde{\Omega}_n]$ and the elements of the $n$ by $n$ matrices are

$$a_{ij} = \left[\{\psi\}_i^*,\ (\beta_1 - \beta)\{\psi\}_j\right]_S + \left[\{\psi\}_i^*,\ (\mathcal{L}_1 - \mathcal{L})\{\psi\}_j\right]_V \qquad (27)$$

$$\lambda_{ij} = \begin{cases} 0 & \text{for } i \neq j \\ \lambda_i & \text{for } i = j \end{cases} \qquad (28)$$

$$b_{ij} = \left[\{\psi\}_i^*,\ [W]_1\{\psi\}_j\right]_V \qquad (29)$$

Therefore, problem (21) is reduced to the standard algebraic eigenvalue problem (26) that can be solved with existing codes [5]. The results of numerical solution for $\widetilde{\Omega}_i$ are to be used in the inversion formula (25) to give the desired eigenfunctions. By increasing the number of terms we can obtain the results with prescribed accuracy.

## CONCLUSION

The theoretical foundations of the unified integral transform method are developed. The method permits to solve numerically a wide class of linear and non-linear engineering problems. The eigenvalues and the eigenfunctions needed can be obtained also by the integral transform method. The solution of several special cases is demonstrated in [5]. Current work is done to extend the application of the method and to create automatic software for heat transfer problems.

## ACKNOWLEDGEMENTS

The authors wish to acknowledge the financial support provided by CNPq/Brasil and kind hospitality of the Mechanical Engineering Dept. at EE/COPPE/UFRJ.

## REFERENCES

[1] PEYROT, R. & TAYLOR, T.D., Computational Methods for Fluid Flow, Springer-Verlag, 1983.

[2] MINKOWYCZ, W.J.; SPARROW, E.M.; SCHNEIDER, G.E. & PLETCHER, R.H. Handbook of Numerical Heat Transfer, John Wiley & Sons, 1988.

[3] MIKHAILOV, M.D. & ÖZIŞIK, M.N. Unified Analysis and Solutions of Heat and Mass Diffusion, John Wiley & Sons, 1984.

[4] MIKHAILOV, M.D. & ÖZIŞIK, M.N. Unified Finite Integral Transform Analysis, Journal of the Franklin Institute, V. 321, 6, 299–307, 1986.

[5] COTTA, R.M. Diffusion-Convection Problems and the Generalized Integral Transform Technique, Núcleo de Publicações, COPPE/UFRJ, 1991.

[6] MIKHAILOV, M.D. Unified Finite Element Analysis, Int. J. Numerical Methods in Engineering, v.19, 1507–1511, 1983.

## OBJETIVO E ESCOPO

A Revista Brasileira de Ciências Mecânicas visa a publicação de trabalhos voltados ao projeto, pesquisa e desenvolvimento nas grandes áreas das Ciências Mecânicas. É importante apresentar os resultados e as conclusões dos trabalhos submetidos de forma que sejam do interesse de engenheiros, pesquisadores e docentes.

O escopo da Revista é amplo e abrange as áreas essenciais das Ciências Mecânicas, incluindo interfaces com a Engenharia Civil, Elétrica, Metalúrgica, Naval, Nuclear, Química e de Sistemas. Aplicacões da Física e da Matemática à Mecânica também serão consideradas.

Em geral, os Editores incentivam trabalhos que abranjam o desenvolvimento e a pesquisa de métodos tradicionais bem como a introdução de novas idéias que possam potencialmente ser aproveitadas na pesquisa e na indústria.

---

## AIMS AND SCOPE

The Journal of the Brazilian Society of Mechanical Sciences is concerned primarily with the publication of papers dealing with design, research and development relating to the general areas of Mechanical Sciences. It is important that the results and the conclusions of the submitted papers be presented in a manner which is appreciated by practicing engineers, researchers, and educators.

The scope of the Journal is broad and encompasses essential areas of Mechanical Engineering Sciences, with interfaces with Civil, Eletrical, Metallurgical, Naval, Nuclear, Chemical and System Engineering as well as with the areas of Physics and Applied Mathematics.

In general, the Editors are looking for papers covering both development and research of traditional methods and the introduction of novel ideas which have potential application in science and in the manufacturing industry.

Notes and Instructions To Contributors

1. The Editors are open to receive contributions from all parts of the world; manuscripts for publication should be sent to the Editor-in-Chief or to the appropriate Associate Editor.
2. (i) Papers offered for publication must contain unpublished material and will be refereed and assessed with reference to the aims of the Journal as stated above. (ii) Reviews should constitute an outstanding critical appraisal of published materials and will be published by suggestion of the Editors. (iii) Letters and communications to the Editor should not exceed 400 words in length and may be: Criticism of articles recently published in the Journal; Preliminary announcements of original work of importance warranting immediate publication; Comments on current engineering matters of considerable actuality.
3. Only papers not previously published will be accepted. Authors must agree not to publish elsewhere a paper submitted to and accepted by the Journal. Exception can be made in some cases of papers published in annals or proceedings of conferences. The decision on acceptance of a paper will be taken by the Editors considering the reviews of two outstanding scientists and its originality, and contribution to science and/or technology.
4. All contributions are to be in English or Portuguese. Spanish will also be considered.
5. Manuscripts should begin with the title of the article, including the english title, and the author's name and address. In the case of co-autors, both addresses should be clearly indicated. It follows the abstract; if the paper's language is different from english, an extended summary in this language should be included. Up to five words for the paper are to be given. Next, if possible, should come the nomenclature list.
6. Manuscripts should be typed with double spacing and with ample margins. Material to be published should be submitted in triplicate. Pages should be numbered consecutively.
7. Figures and line drawing should be originals and include all relevant details; only excelent photocopies should be sent. Photographs should be sufficiently enlarged to permit clear reproduction in half-tone. If words or numbers are to appear on a photograph they should be sufficiently large to permit the necessary reduction in size. Figure captions should be typed on a separate sheet and placed at the end of the manuscript.

REVISTA BRASILEIRA DE CIÊNCIAS MECÂNICAS
*JOURNAL OF THE BRAZILIAN SOCIETY OF MECHANICAL SCIENCES*

*Vol. XII - Nº 3* *1990*

## *ÍNDICE / CONTENTS*